J. Fluid Mech. (1979), *vol.* 94, *part* 2, *pp.* 209–242
Printed in Great Britain

The effect of short regions of high surface curvature on turbulent boundary layers

By A. J. SMITS,† S. T. B. YOUNG‡ AND P. BRADSHAW
Department of Aeronautics, Imperial College, London

(Received 21 August 1978)

Measurements, including one-point double, triple or quadruple mean products of velocity fluctuations, have been made in low-speed turbulent boundary layers on flat surfaces downstream of concave or convex bends with turning angles of 20 or 30 degrees, the length of the curved region being at most 6 times the boundary-layer thickness at entry. These short bends approximate to 'impulses' of curvature, and the object of the work was to investigate the impulse response of the boundary layer, essentially the decay of structural changes downstream of the bends. The work can be regarded as a sequel, with much more detailed measurements, to the study by So & Mellor (1972, 1973, 1975) who investigated the response to step increases of curvature: turbulent boundary layers being nonlinear systems, responses to several kinds of curvature history are needed to assemble an adequate description of the flow. The most striking feature of the 'impulse' response is that the decay of the high turbulent intensity found at exit from the concave bends is not monotonic; the Reynolds stresses in the outer layer collapse to well below the level at entry, and are still falling slowly at the end of the test rig although in principle they must recover eventually. On the convex (stabilized) side the flow recovers, monotonically in the main, from a low level of turbulent intensity at the exit. The pronounced second-order response on the concave side can be explained qualitatively by interaction between the shear stress and the mean shear and is not peculiar to curved flows, but in the present cases the response is complicated by large changes in the dimensionless structure parameters related to double or triple mean products of velocity fluctuations. Strong spanwise variations, due presumably to longitudinal vortices, further complicate the flow in the concave bends, and decay only very slowly downstream.

1. Introduction

This paper is one of a series on 'complex' turbulent flows (defined as shear layers with complicating influences like distortion by extra rates of strain or interaction with another turbulence field). General reviews of complex flows are given by Bradshaw (1975, 1976). The latter paper outlines the Imperial College research programme, whose final goal is the improvement of calculation methods for turbulent flows of interest to engineers; virtually all of these flows are recognizable as shear layers even if they change too rapidly to satisfy the thin-shear-layer ('boundary-layer') approximation. Examples of extra rates of strain, additional to the simple shear $\partial U/\partial y$ that

† Present address: Mechanical Engineering Department, University of Melbourne.
‡ Present address: Nuclear Engineering Department, Queen Mary College, London.

0022–1120/79/4261–7230 $02.00

drives the shear layer, include lateral divergence $\partial W/\partial z$, discussed in the companion paper by Smits, Eaton & Bradshaw (1979; hereafter cited as II), and streamline curvature in the plane of the simple shear, $\partial V/\partial x$. Streamline curvature can be imposed either by rotation of the whole system (e.g. Johnston, Halleen & Lezius 1973; Lezius & Johnston 1976; Koyama *et al.* 1978) or by the boundary geometry in a non-rotating flow. In all cases the interest is in the effect of the distortion on the dimensionless parameters describing the turbulence structure (hereafter called the 'structure') and thus on the dimensionless constants or functions appearing in methods for calculating dimensional properties such as Reynolds stress.

Streamline curvature is probably the commonest example of an extra strain rate, and the effects of prolonged streamline curvature, leading to the establishment of a new near-equilibrium turbulence structure, have been studied by many experimenters. Publications since the review by Bradshaw (1973) include So & Mellor (1973, 1975) and So (1975), whose work will be discussed in some detail below, and Meroney & Bradshaw (1975) whose measurements in 25° bends with radii of about 100 times the thickness of the initial boundary layer have been continued by Hoffmann & Bradshaw (1978) and paralleled and extended by Ramaprian & Shivaprasad (1978). Guitton & Newman (1977) have presented Reynolds-stress measurements in wall jets on convex surfaces.

Although the effects of prolonged streamline curvature are by no means fully understood, study of the effect of sudden changes in curvature is justified because of their frequency of occurrence in practice and because the step response or impulse response of a system, even a nonlinear one, should help to illuminate the 'steady-state' behaviour. The present results, indeed, provide a spectacular proof that a turbulent shear layer behaves like a second-order system with sub-critical damping. The response of a given flow to a true impulse of curvature – that is, an infinitely rapid deflexion of the flow through a given angle – must be a function only of the angle, as in the case of Taylor–Görtler instability (Tobak 1971): therefore we expect the response to a short region of finite curvature to depend mainly on the total turning angle and not on the radius of curvature as such. Of course, the state of the turbulence at exit from a short bend (initial response to a curvature impulse) will still be far from the equilibrium state it would reach if the bend continued indefinitely at the same curvature (asymptotic response to a step-change in curvature). The present measurements for an approximation to a curvature impulse in the rig shown in figure 1 may be regarded as a more detailed sequel to the measurements by So & Mellor (1972, 1973, 1975; the second and third papers are updated excerpts from the first) downstream of step *increases* in curvature. The states of the flow at exit from the 30° bends with $\delta/R \simeq 0{\cdot}085$–$0{\cdot}17$ used in the present work are roughly the same as the near-asymptotic states reached in So & Mellor's measurements with $\delta/R \simeq 0{\cdot}035$–$0{\cdot}05$, the two figures for δ/R being for the concave and convex sides respectively. The ratio of the extra strain rate to the mean shear is about the same in the present experiments on a convex surface as in the measurements of Castro & Bradshaw (1976) in a mixing layer with a short region of stabilizing curvature, but in the latter case the deflexion angle was 90 degrees compared to 20 or 30 degrees in the present work.

In the rig shown in figure 1, boundary layers which have developed on flat surfaces encounter short regions of large surface curvature, of either sign, and then relax again on flat surfaces. There are small favourable pressure gradients over the flat surfaces

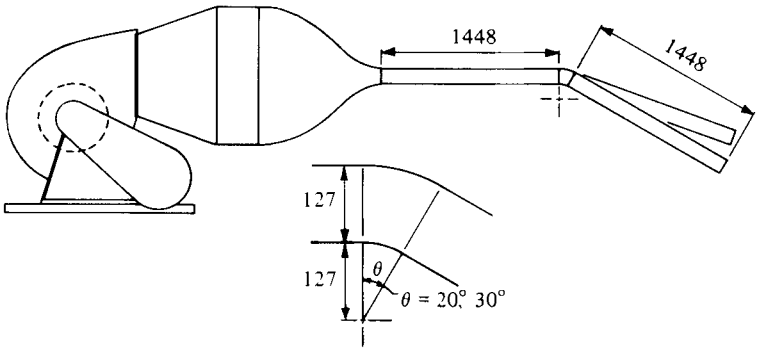

FIGURE 1. General arrangement of test rig. Dimensions in mm.

and large pressure gradients of either sign in the curved regions, but pressure gradients do not appear directly in the Reynolds-stress transport equations and are therefore unlikely to affect the turbulence structure directly. No detailed measurements were made within the bends because the object was to simulate a curvature impulse, but approximate skin-friction measurements with Preston tubes confirm that the boundary layers were far from separation everywhere. The use of a sharper bend would have involved some danger of separation, at least in the corners of the test rig, but the results show that the present bend was not sharp enough to simulate a curvature impulse accurately in the concave case. The increase in shear stress τ, and therefore in $\partial\tau/\partial y$, within the concave bends is so large that the total pressure on a given streamline changes significantly between entry and exit, a distance of about 6δ: thus, the velocity profile at exit from the bend, where the static pressure becomes uniform again, is already significantly different from the entry profile. In the case of a true impulse, the shear stress and other turbulence properties would change instantaneously and the change in total pressure would follow more slowly. On the convex side of the bend the shear stress in the outer layer is greatly reduced and the velocity profile is therefore almost frozen for $y/\delta > 0{\cdot}4$. The failure to simulate an impulse of curvature accurately does not seriously complicate the qualitative interpretation of the results and is of no consequence in quantitative comparisons with calculation methods.

The 20 degree concave bend has the same shape in side view as the cylinder-flare body of revolution tested in II. The latter experiment was intended primarily as an investigation of lateral-divergence effects, but it is impossible to pass from an axial flow to a laterally diverging one without either three-dimensional effects (on a flat surface) or surface curvature (if a body of revolution is used) and the latter was accepted as the lesser evil. Therefore the 20 degree plane-bend flow was set up so that the effects of surface curvature could be studied separately. The original hope was that the curvature effects would die out quickly enough downstream of the bend that the effects of divergence alone could be deduced by subtracting the residual curvature effects (measured in two-dimensional flow) from the measurements on the body of revolution. The long persistence of curvature effects complicates matters, but a comparison of the two-dimensional and axisymmetric results is still instructive and is undertaken in II.

The results of the present experiment, summarized in figure 2 for the 30 degree bend, show extremely large effects of surface curvature. The shear stress at exit from

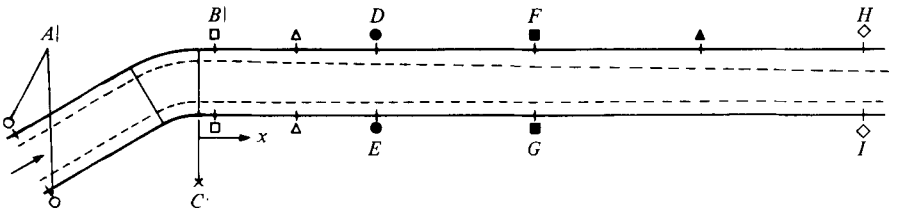

FIGURE 2. Positions of traverse stations and key to results (30° bend only). A, $\tau \simeq 0{\cdot}001$, $a_1' \simeq 0{\cdot}13$, $V_q \to 0{\cdot}015$; B, $\tau \simeq 0{\cdot}0025$, $a_1' \simeq 0{\cdot}2$, $V_q \to 0{\cdot}04$; C, $\tau \simeq 0$, $a_1' \simeq 0$, $V_q \to 0{\cdot}001$; D, $\tau \simeq 0{\cdot}0005$, $a_1' \simeq 0{\cdot}12$, $V_q \to 0{\cdot}02$; E, $\tau \simeq 0{\cdot}0005$, $a_1' \simeq 0{\cdot}13$, $V_q \to 0{\cdot}002$; F, $\tau \simeq 0{\cdot}0002$, $a_1' \simeq 0{\cdot}09$, $V_q \to 0{\cdot}015$; G, $\tau \simeq 0{\cdot}001$, $a_1' \simeq 0{\cdot}14$, $V_q \to 0{\cdot}004$; H, $\tau \simeq 0{\cdot}00015$, $a_1' \simeq 0{\cdot}06$, $V_q \to 0{\cdot}013$; I, $\tau \simeq 0{\cdot}001$, $a_1' \simeq 0{\cdot}14$, $V_q \to 0{\cdot}015$. τ, a_1' are dimensionless shear stress and stress/energy ratios at $y = 0{\cdot}5\delta$: V_q is energy transport velocity at $y \simeq \delta$.

the bends is of the same order as that predicted by the linear correction formulae (Bradshaw 1973) devised for small curvature effects, whereas we had expected that strong self-limiting nonlinearities ('stiff' response) would occur. In the 30 degree concave bend the shear stress at $y/\delta \simeq 0{\cdot}4$ increases by a factor between 2·2 and 5·5 (depending on spanwise position) in a streamwise distance of 6δ. The large shear-stress gradients normal to the surface greatly reduce $\partial U/\partial y$ in the outer part of the layer, so that after the end of the regions of destabilizing curvature the generation term in the shear-stress transport equation, $\overline{v^2}\,\partial U/\partial y$, falls rapidly below its equilibrium value, leading to a fall in the shear stress and hence, via the turbulent energy equation, in $\overline{u^2}$, $\overline{w^2}$, and $\overline{v^2}$ which produces a further fall in shear stress. There are also large changes in the dimensionless structure parameters. Recovery is extremely slow. The large spanwise variations found at the bend exit persist as the flow proceeds downstream; only limited measurements of flow direction have been made but indirect measurements strongly suggest that the longitudinal vortices found by other workers are formed in the bend and persist almost indefinitely downstream. Results for the 20 degree concave bend are similar but less spectacular. At exit from the 30 degree *convex* bend the shear stress in the outer layer is very small, but since, as a result, $\partial U/\partial y$ is nearly the same as at entry to the bend, and since $\overline{v^2}$ is only a factor of two or three less than at entry, regeneration of shear stress is comparatively rapid: further downstream, the shear stress and intensity rise above the values at entry to the bend, although in contrast to the concave cases the structural parameters appear to return monotonically to the undisturbed values. This behaviour is similar to that of Castro & Bradshaw's (1976) mixing layer.

The tendency of the longitudinal vortices to persist is aggravated by the collapse of the turbulence downstream of the concave bends, leading to very low mixing rates. As a result the flow, even at the end of the test rig, is far from two-dimensional and complete mapping in cross-sectional planes would be needed to define it. This was not expected when the experiment was planned, and we felt that such exhaustive measurements would not be justified until the process of triggering the vortices was better understood and if possible controlled.

The results as they stand provide useful information for the development or testing of calculation methods for highly curved surfaces but further work on this subject, and on the application of conditional-sampling techniques to the further study of mean and fluctuating longitudinal vortices in curved flows, will be reported separately.

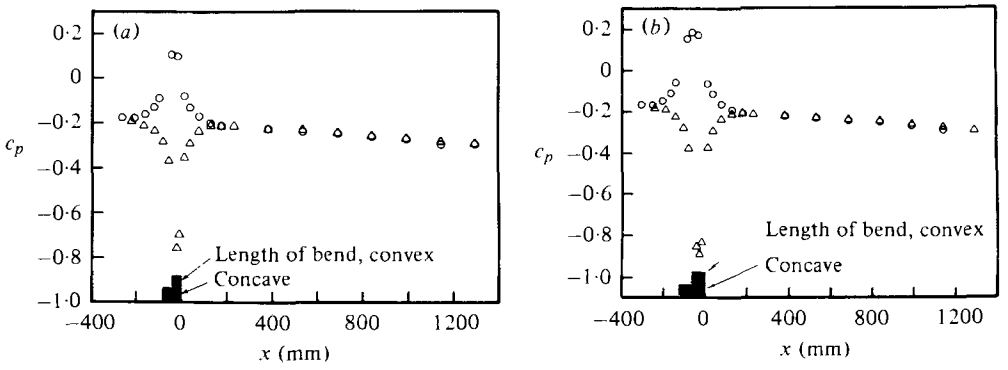

FIGURE 3. Surface pressure distributions. (*a*) 20° bend; (*b*) 30° bend. ○, concave side; △, convex side.

Section 2 describes the apparatus and techniques, while § 3 presents the results, with some preliminary discussion of velocity and shear stress profiles. Section 4 demonstrates analytically that the non-monotonic recovery of the shear stress and velocity profiles downstream of the curved region is a universal feature of turbulent shear layers and not a special consequence of structural changes induced by curvature. Section 5 is a detailed discussion of the results, including intensities, triple products and structure parameters, while § 6 continues the discussion with special reference to calculation methods. More detailed results and discussion are presented by Smits, Young & Bradshaw (1978; hereafter cited as A).

2. Apparatus and techniques

The test rig, shown in figure 1, consists of a duct 762 mm wide and 127 mm high, supplied from the blower-contraction unit described by Bradshaw (1972). The nominal flow speed, used as a reference velocity and denoted by U_{ref} below, was about 32 m s^{-1} ($U_{\mathrm{ref}}/\nu \simeq 2{\cdot}1 \times 10^6$ m^{-1}) for all measurements reported here. Because of boundary-layer growth, the free-stream velocity increases by about 5 per cent between the contraction exit and the entry to the bend, a distance of 1448 mm (values of pressure coefficient in figure 3 are relative to the static pressure at the point of measurement of U_{ref}, slightly inside the contraction; at the contraction exit, c_p is roughly $-0{\cdot}07$). The pressure-gradient parameter $(\delta^*/\tau_w)\,dp/dx$ just before the bend is only about $-0{\cdot}05$, and the skin friction coefficient is negligibly different from the expected value of 0·00295 for a constant-pressure flow at the local Reynolds number $U_e\theta/\nu$ of about 6000; the Coles wake parameter Π is about 0·50. Low-Reynolds-number effects on the velocity-defect profile and the turbulence structure in the outer layer should have been negligible, at least at entry to the bend.

The bend radii were 127 mm on the convex side and 254 mm on the concave side, approximately 6 and 12 times the boundary-layer thickness δ_{995} at entry, $\delta_0 \simeq 21$ mm. Bend angles of 10, 20 or 30 degrees could be set by interchangeable shaped blocks, and the bends were followed by another 127 mm high section, of length 1448 mm or about $66\delta_0$. Since the ratio of duct width to boundary-layer thickness at the bend was about 36 and the flow in the centre-plane was far from separation, no boundary-layer

Case	Symbol	x (mm)	δ_{995} (mm)	U_e/U_{ref}
Concave, 30 deg., $C_{f,max}$ (CC30C)	○	−251	21·87	1·071
	□	30	28·40	1·079
	△	183	31·30	1·100
	●	335	34·29	1·106
	■	635	39·56	1·118
	▲	945	44·15	1·127
	◇	1250	45·89	1·149
Concave, 30 deg., $C_{f,min}$ (CC30T)	○	−251	21·87	1·071
	□	4	31·91	1·079
	△	157	36·10	1·100
	●	310	40·88	1·106
	▲	919	55·20	1·127
Concave, 20 deg., $C_{f,max}$ (CC20C)	○	−234	18·79	1·071
	□	4	22·49	1·040
	△	157	24·70	1·087
	●	310	26·78	1·092
	▲	919	34·66	1·112
Convex, 30 deg. (CV30)	○	−185	21·88	1·105
	□	30	23·64	1·114
	△	183	25·15	1·102
	●	335	26·61	1·106
	■	635	29·35	1·115
	◇	1250	36·32	1·138

TABLE 1. Free-stream velocity, boundary-layer thickness δ_{995} and symbol key.

control devices were fitted to limit secondary flow near the side walls in the bend region.

The measurement techniques used are described in A and were generally conventional. Mean velocities were measured with Pitot tubes and turbulence quantities with constant temperature hot-wire anemometers; hot-wire signals were recorded on analogue magnetic tape and later transcribed to digital tape for batch processing (including linearization).

The measurements were intended mainly to permit evaluation of the terms in the transport equation for the Reynolds shear stress $-\rho\overline{uv}$, and full w component measurements were not made.

During the course of the measurements the wind-tunnel inlet filter and screens were occasionally cleaned and towards the end of the work the wide-angle diffuser was shortened from the arrangement described by Bradshaw (1972) to that shown in figure 1. These changes affected the spanwise distribution of skin friction, notably downstream of the concave bends, but each data set is self-consistent and the corresponding skin friction distributions are plotted in figure 6.

3. Results and preliminary discussion

Four sets of results are presented below. More details are given in A and tabulations are available from the authors at Imperial College. Concave-surface flows exhibit strong spanwise variations and, for the 30 degree bend, complete sets of data were recorded in two streamwise planes at one maximum and one minimum point

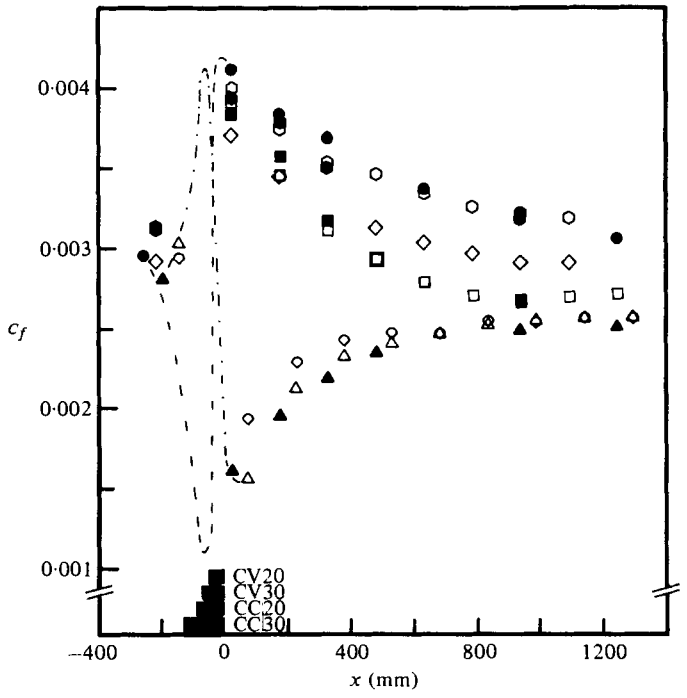

FIGURE 4. Skin-friction coefficients, based on pseudo-free-stream velocity U_e. Open symbols from Preston tube; full symbols from logarithmic velocity profiles. 20° bend: ○, concave (crest), CC20C; ◇, concave (trough), CC20T; ▽, convex, CV20. 30° bend: ○, concave (crest), CC30C; □, concave (trough), CC30T; △, convex, CV30. Approximate Preston-tube measurements within 30° bend: – – –, concave; – · –, convex. Bars ending at $x = 0$ show bend lengths.

on the spanwise distribution of surface shear stress, the spanwise distance between the two measurement planes being 25 mm or about 1·2 times the initial boundary-layer thickness. Adopting So & Mellor's convention of referring to the positions of the maximum and minimum c_f as the 'crest' and 'trough' respectively, the four main cases are coded as follows:

CC30C (ConCave bend, 30 degree turning angle, at Crest position);
CC30T (ConCave bend, 30 degree turning angle, at Trough position);
CC20C (ConCave bend, 20 degree turning angle, at Crest position);
CV30 (ConVex bend, 30 degree turning angle, spanwise position immaterial).

Except for mean velocity profiles and skin-friction coefficient, the results are made dimensionless with U_{ref} and δ_{995} (the value of y at which $U = 0{\cdot}995U_e$, hereafter referred to as 'δ'). Values of U_e/U_{ref} and δ (mm) are given in table 1.

The following further conventions are used: the first measurement station, 120–140 mm upstream of the start of the bend according to the case considered, is called the 'entry'; the second station, 4 or 30 mm downstream of the origin of co-ordinates at the end of the bend, is called the 'exit'; the 'last measurement station' is at $x = 1250$ mm for CC30C and CV30 and at $x = 919$ mm for the other two cases. The words 'convex' and 'concave' are used to distinguish the flows even when the discussion relates to the flat surfaces downstream of the bends.

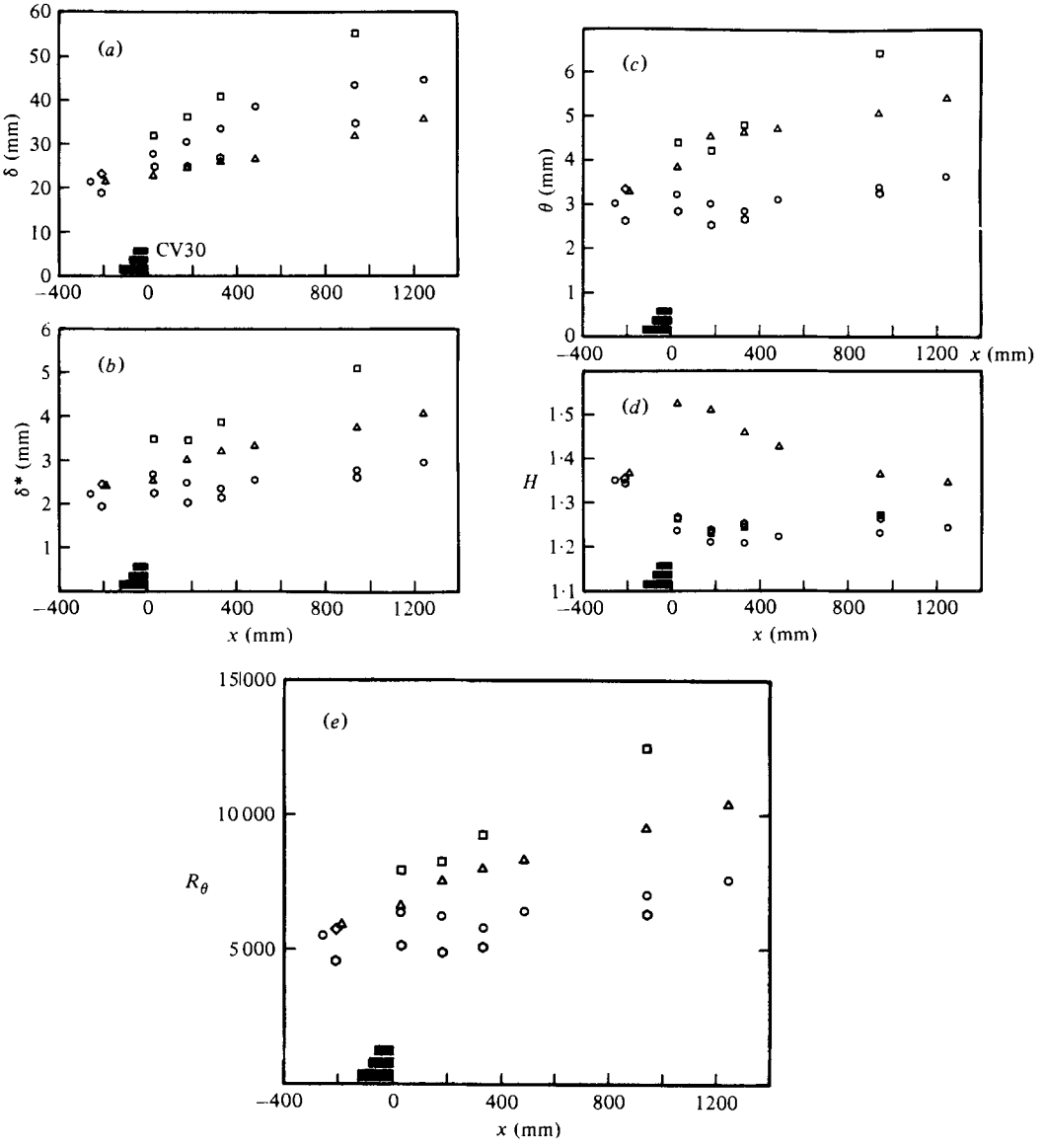

FIGURE 5. Integral properties. Symbols as in figure 4: ○, CC30C; □, CC30T; ○, CC20C; △, CV30. (*a*) Total thickness δ_{995}; (*b*) displacement thickness δ^*; (*c*) momentum thickness θ; (*d*) shape parameter $H = \delta^*/\theta$; (*e*) momentum-thickness Reynolds number $U_e\theta/\nu$.

3.1. *Integral parameters*

The skin-friction coefficient $c_f = \tau_w/\frac{1}{2}\rho U_e^2$ is plotted against x in figure 4. The dotted lines within the bend region are approximate Preston tube values for CC30C and CV30, obtained at an early stage in the work and intended for guidance only: the variation within the bend is broadly the expected response to pressure gradient. It is seen at once that the most downstream values at $x \simeq 1250$ mm are still far from the constant-pressure values for the corresponding $U_e\theta/\nu$, which differs from case to case: the pressure gradient in the downstream part of the duct is small, and virtually the same

CC30C						
x (mm)	25	178	330	483	940	1245
c_p	−0·112	−0·209	−0·224	−0·236	−0·267	−0·297
$\frac{1}{2}c_f \times 10^3$	2·058	1·918	1·843	1·685	1·598	1·528
$10^3\theta/(x-x_0)$	−4·814	2·385	1·508	0·900	0·675	1·009
$x-x_0$ (mm)	−555	1044	1550	2821	4080	2910
CC30T						
x (mm)	28	180	333	—	942	—
c_p	−0·105	−0·210	−0·225	—	−0·267	—
$\frac{1}{2}c_f \times 10^3$	1·914	1·788	1·583	—	1·340	—
$10^3\theta/(x-x_0)$	−7·102	−1·000	−0·945	—	−1·442	—
$x-x_0$ (mm)	−489	−3431	−4083	—	−3532	—
CC20C						
x (mm)	28	180	333	—	942	—
c_p	−0·113	−0·216	−0·232	—	−0·273	—
$\frac{1}{2}c_f \times 10^3$	1·567	1·956	1·747	—	1·590	—
$10^3\theta/(x-x_0)$	−4·763	1·545	0·826	—	0·561	—
$x-x_0$ (mm)	−467	1316	2960	—	4608	—
CV30						
x (mm)	25	178	330	483	940	1245
c_p	−0·330	−0·211	−0·219	−0·230	−0·259	−0·288
$\frac{1}{2}c_f \times 10^3$	0·806	0·976	1·094	1·172	1·244	1·252
$10^3\theta/(x-x_0)$	0·379	−0·532	−0·242	−0·040	−0·065	−0·177
$x-x_0$ (mm)	6353	5658	13150	58580	57430	22780

TABLE 2. Virtual origin of lateral convergence/divergence: $\theta/(x-x_0)$ assumed equal to $\frac{1}{2}c_f-(\theta/U_e)\,(H+2)\,dU_e/dx-d\theta/dx$, where $U_e/U_{ref} = (1-c_p)^{\frac{1}{2}}$.

in all cases, so that the differences between the concave and convex sides downstream of the bends are due almost entirely to the long-lasting effects of surface curvature.

The boundary-layer thicknesses and shape parameter H are plotted in figure 5. Note that the boundary-layer thickness is a minimum at the 'crest' (maximum in c_f) and a maximum at the 'trough'. As usual, the trend in H is opposite to the trend in c_f, and the only point to be noted at present is the very large change in H through the bend, implying that most of the velocity profile, and not merely c_f or the velocity close to the surface, is affected; this in turn implies large shear-stress gradients, within the bend, over most of the boundary-layer thickness.

Since the pressure gradient downstream of the bend is small, differences between $d\theta/dx$ and $\frac{1}{2}cf$ imply three-dimensional effects. Table 2 gives the imbalance in the momentum integral equation at each measurement station; if convergence/divergence were collinear and all measurement errors and neglected terms negligible, this would be equal to $\theta/(x-x_0)$ where x_0 is the virtual origin of the divergence. Even when the cross-flow is non-collinear, as in the present concave cases (at least), $x-x_0$ is still a useful quantity for semi-quantitative assessment. The convex case has mild convergence (virtual origin about 20 m downstream of the test section), attributable to secondary flows, generated within the bend, on the end walls. The concave cases have lateral divergence at the crest and convergence at the trough, as expected if the spanwise variations are caused by pairs of longitudinal vortices ($V < \overline{V}$, $\partial W/\partial z > 0$ at the crest in $c_f(z)$, $V > \overline{V}$ at the trough one-half wavelength to the side).

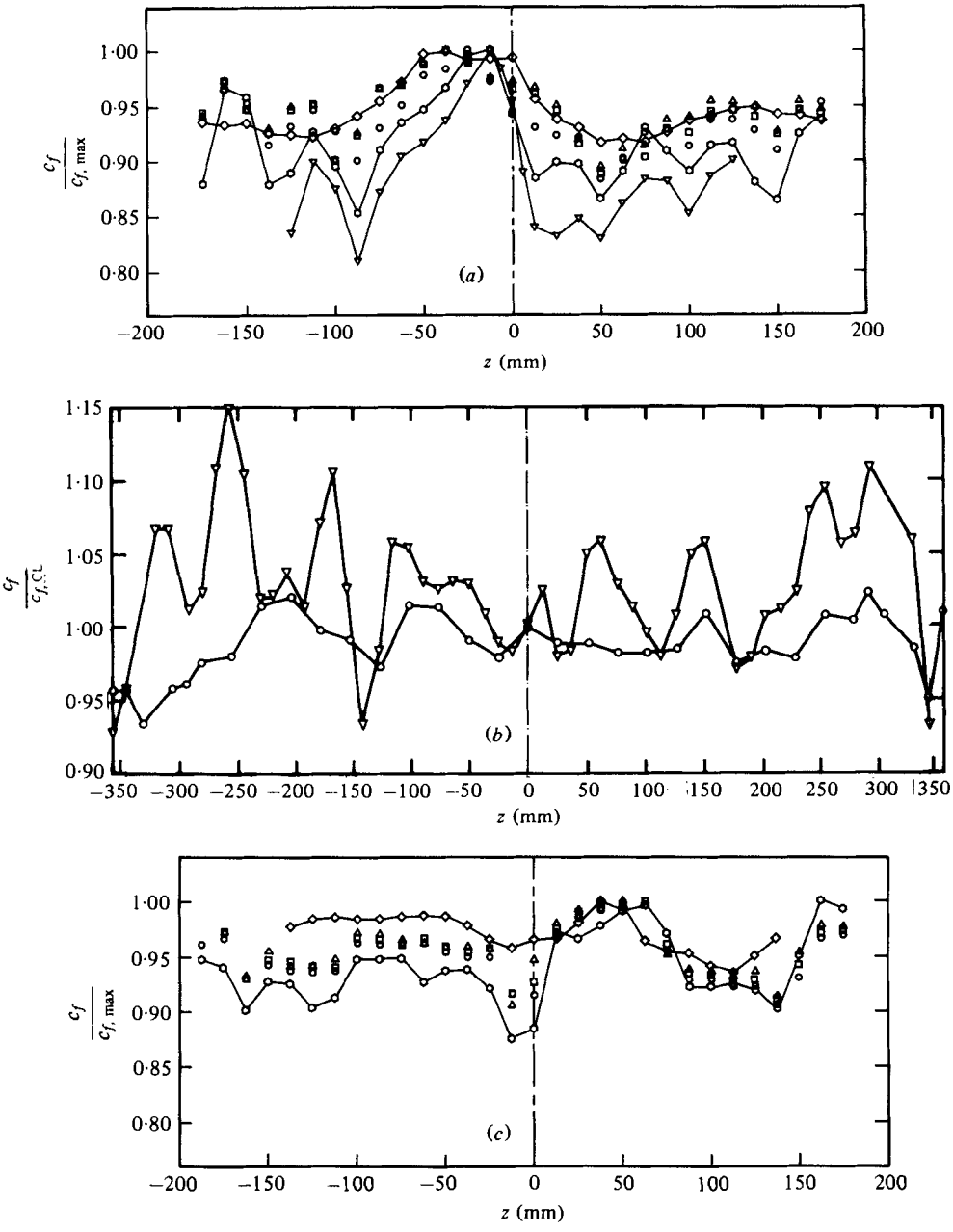

FIGURE 6 (*a*, *b*, *c*). For legend see p. 221.

Figure 6, in which most quantities are normalized by their maximum values with respect to z, shows the spanwise variations of the skin-friction coefficient (measured with Preston tubes) and other quantities. Figure 6 (*a*) shows how the c_f pattern changes through the 20° and 30° concave bends; here the downstream readings are roughly 8 boundary-layer thicknesses from the bend exit. The upstream pattern, imposed by inevitable irregularities of weave in the wind-tunnel damping screens, obviously has some effect on the shape of the downstream pattern – although the dominant

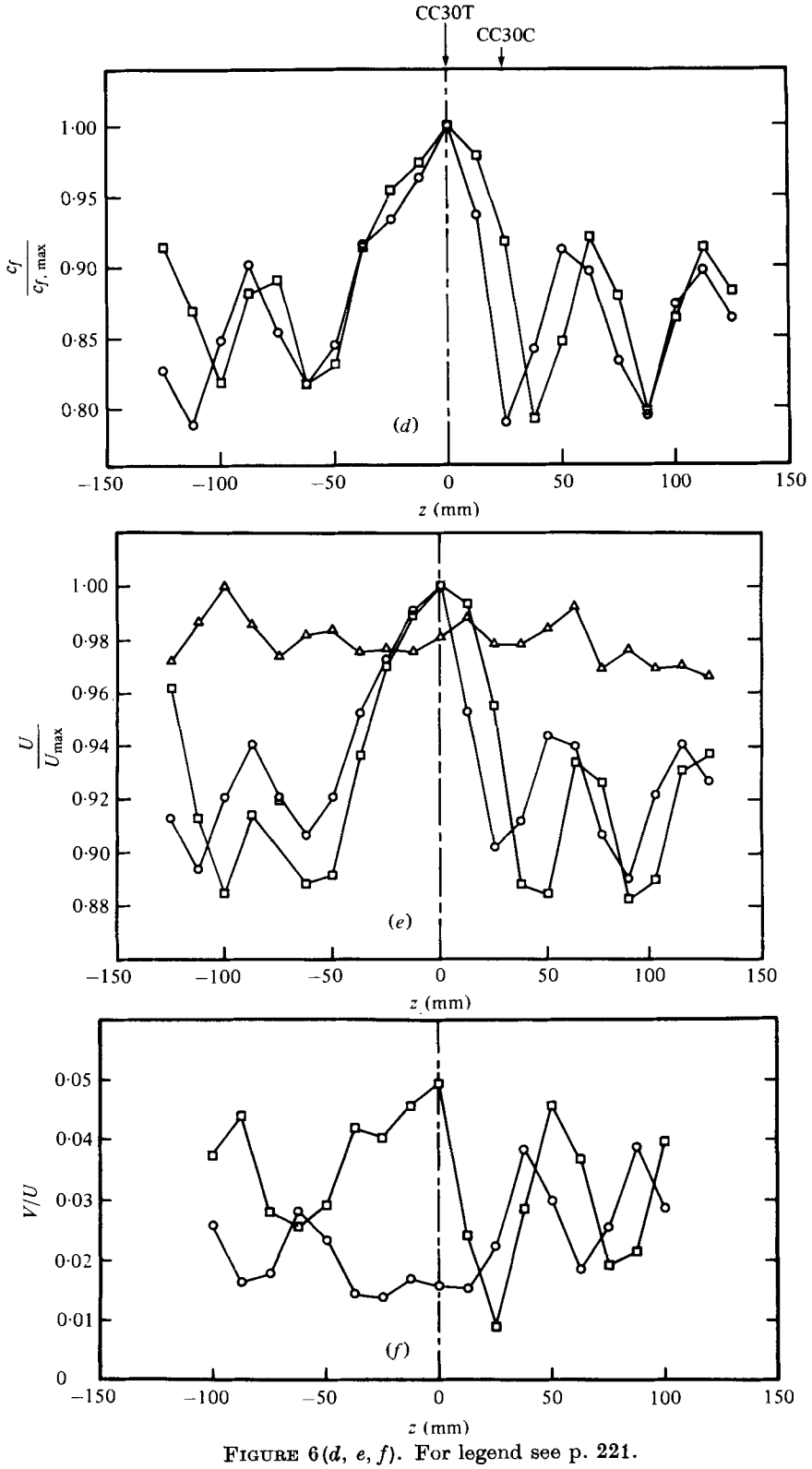

FIGURE 6(*d*, *e*, *f*). For legend see p. 221.

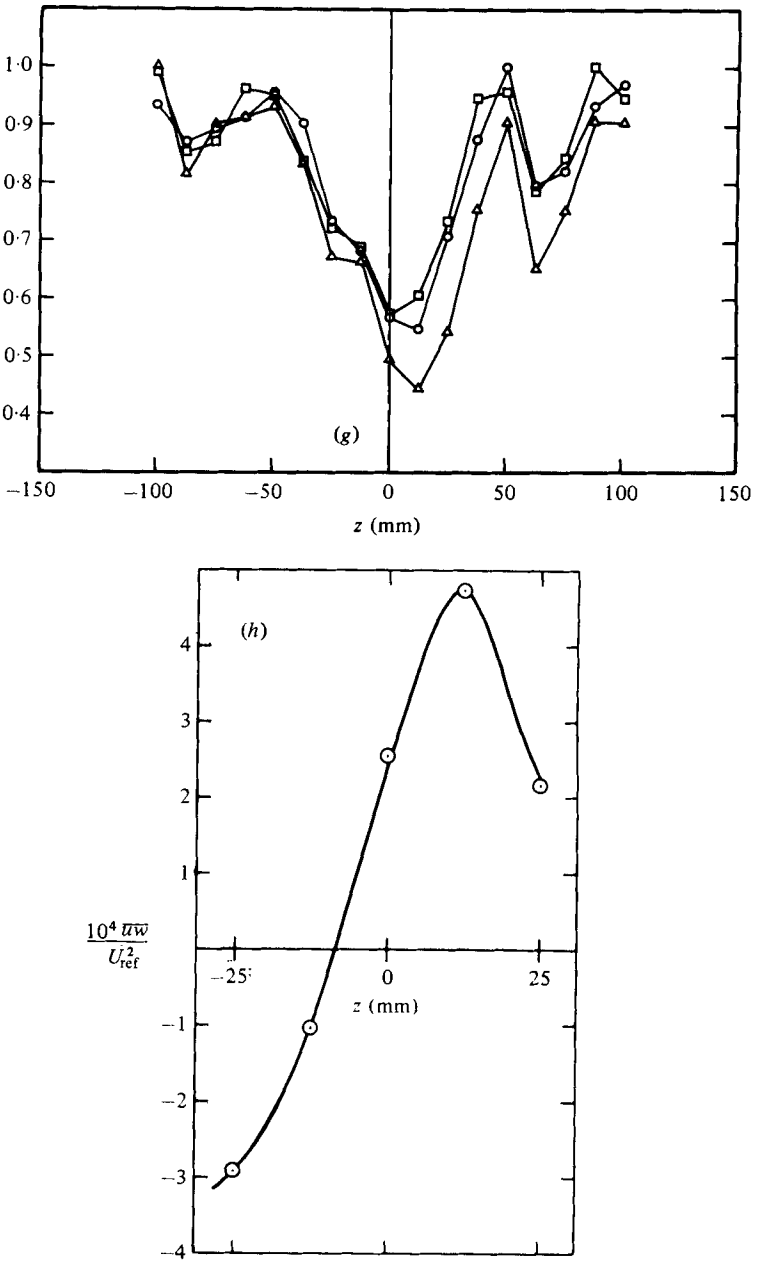

FIGURE 6(*g*, *h*). For legend see opposite page.

wavelength is set by the boundary-layer thickness – but the amplitude of the pattern depends mainly on the bend angle. This is shown by figure 6(*b*); recently the metal screens were replaced by polyester ones of nearly the same open-area ratio, about 0·58, which reduced the amplitude of the upstream pattern by a factor of about two, while the amplitude of the downstream pattern was nearly as large as before. Figure 6(*c*) compares the effect of concave and convex bends of 20 degree angle: these measurements were made on the floor of the tunnel (the convex side in the

main measurements). A convex bend actually *reduces* the spanwise variations caused by the tunnel screens. This is not necessarily expected, and strongly suggests that the screen-induced disturbances are themselves longitudinal vortices, as hypothesized by Bradshaw (1965): if this is so the convex bend would attenuate the vortices, and ordinary turbulent mixing would then efface the spanwise variations – apparently quite rapidly.

Figure 6(*d*) shows how the pattern persists, almost unaltered, downstream of the bend. This pattern corresponds to the main sets of results for CC30C ($z = 0$) or CC30T ($z = 25$ mm; the trough was *not* tracked as it drifted across the tunnel with increasing x). The upstream pattern corresponding to these results (and to CC20C) was closely similar to that for $x = -260$ mm in figure 6(*a*) but translated across the test rig so that its main peak occurred at $x = 0$. Figure 6(*e*) shows the mean velocity patterns at $y \simeq 0{\cdot}25\delta$ at the same x positions as the c_f patterns in figure 6(*d*), which they closely resemble. One must not too quickly deduce that the flow at a given z position is quasi-two-dimensional, obeying the usual relations between velocity-profile shape and c_f: however it is fair to infer that the longitudinal vortices which maintain the spanwise variations do not greatly affect the structure of the inner layer. The peak-to-peak variations of U and c_f are of the order of 10 and 20 per cent, but figure 6(*g*) shows very much larger variations in the Reynolds stresses, in antiphase with c_f. At $x = 1415$ mm, δ varies between about 45 and 60 mm and so the spanwise wavelength of the above-mentioned quantities is roughly equal to the local boundary-layer thickness. The wavelength is of course set in the bend, where δ is of the order of 25 mm, so that the preferred wavelength is roughly twice the entry boundary-layer thickness, as would be expected if the basic pattern was a pair of contra-rotating vortices with a diameter only slightly less than δ. There is perhaps some slight evidence from figures 6(*c*) and 6(*d*) that alternate peaks are starting to disappear at $x \simeq 1400$ mm, restoring the original ratio of wavelength to boundary-layer thickness: this effect is often found in measurements of disturbances introduced (on plane surfaces) by wind-tunnel screens (e.g. Fernholz 1962).

3.2. *Profiles*

The distortions of the mean-velocity profiles, Reynolds stress profiles and structural parameters presented in figures 7–15 are so spectacular that a brief overall description

FIGURE 6. Spanwise variations: most quantities except skewness and flatness normalized by local maxima. Figures 6(*d–l*) refer to 30° concave bend (CC30), mainly at $x \simeq 170$ and/or 1400 mm. (*a*) Effect of concave bends on c_f (patterns corresponding to main concave-surface results are similar but displaced about 25 mm in positive z position). □, upstream ($x = -260$ mm); ○, downstream of 20° bend ($x = 173$ mm); ▽, downstream of 30° bend ($x = 168$ mm). (*b*) Effect of concave bend on c_f, normalized by centre-line values: screens replaced. ○, upstream; ▽, 30° bend, downstream ($x \simeq 1500$ mm). (*c*) Effect of 20° concave and convex bends on c_f (lower surface; convex side in main results). □, upstream ($x = -271$ mm); ○, downstream of concave bend ($x = 160$ mm); ◇, downstream of convex bend ($x = 160$ mm). (*d*) Persistence of c_f pattern downstream of 30° concave bend (as in main results). ○, $x = 168$ mm; □, $x = 1415$ mm. (*e*) U-component mean velocity pattern at $y \simeq 0{\cdot}25\delta$ downstream of 30° concave bend. ○, $x = 168$ mm, $y = 8{\cdot}9$ mm; □, $x = 1415$ mm, $y = 12{\cdot}5$ mm; △, convex bend, $x = 170$ mm, $y = 7{\cdot}1$ mm. (*f*) V-component mean velocity pattern at $y \simeq 0{\cdot}25\delta$ downstream of 30° concave bend. □, $x = 168$ mm, $y = 8{\cdot}9$ mm; ○, $x = 1415$ mm, $y = 12{\cdot}5$ mm. (*g*) Reynolds-stress pattern at $y \simeq 0{\cdot}25\delta$ downstream of 30° concave bend, $x = 1382$ mm, $y = 12{\cdot}6$ mm. ○, $\overline{u^2}$; □, $\overline{v^2}$; △, $-\overline{uv}$. (*h*) Transverse shear stress, $x = 945$ mm, $y = 3{\cdot}9$ mm ($y/\delta \sim 0{\cdot}09$).

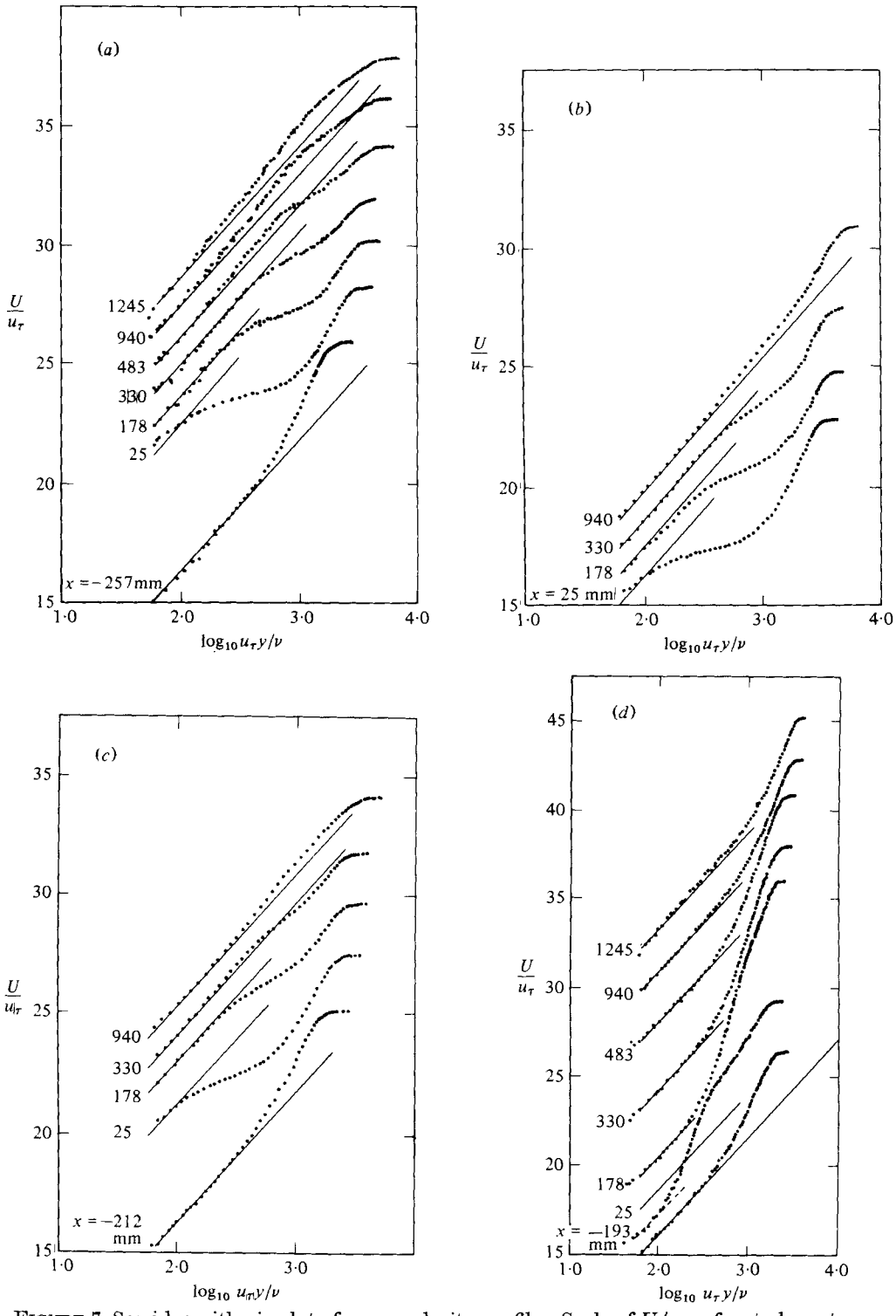

FIGURE 7. Semi-logarithmic plot of mean velocity profiles. Scale of U/u_τ refers to lowest curves; left-hand end of log-law line marks $U/u_\tau = 15$ for other curves, the upward shifts being multiples of 1·25 units. (*a*) CC30C; (*b*) CC30T; (*c*) CC20C; (*d*) CV30.

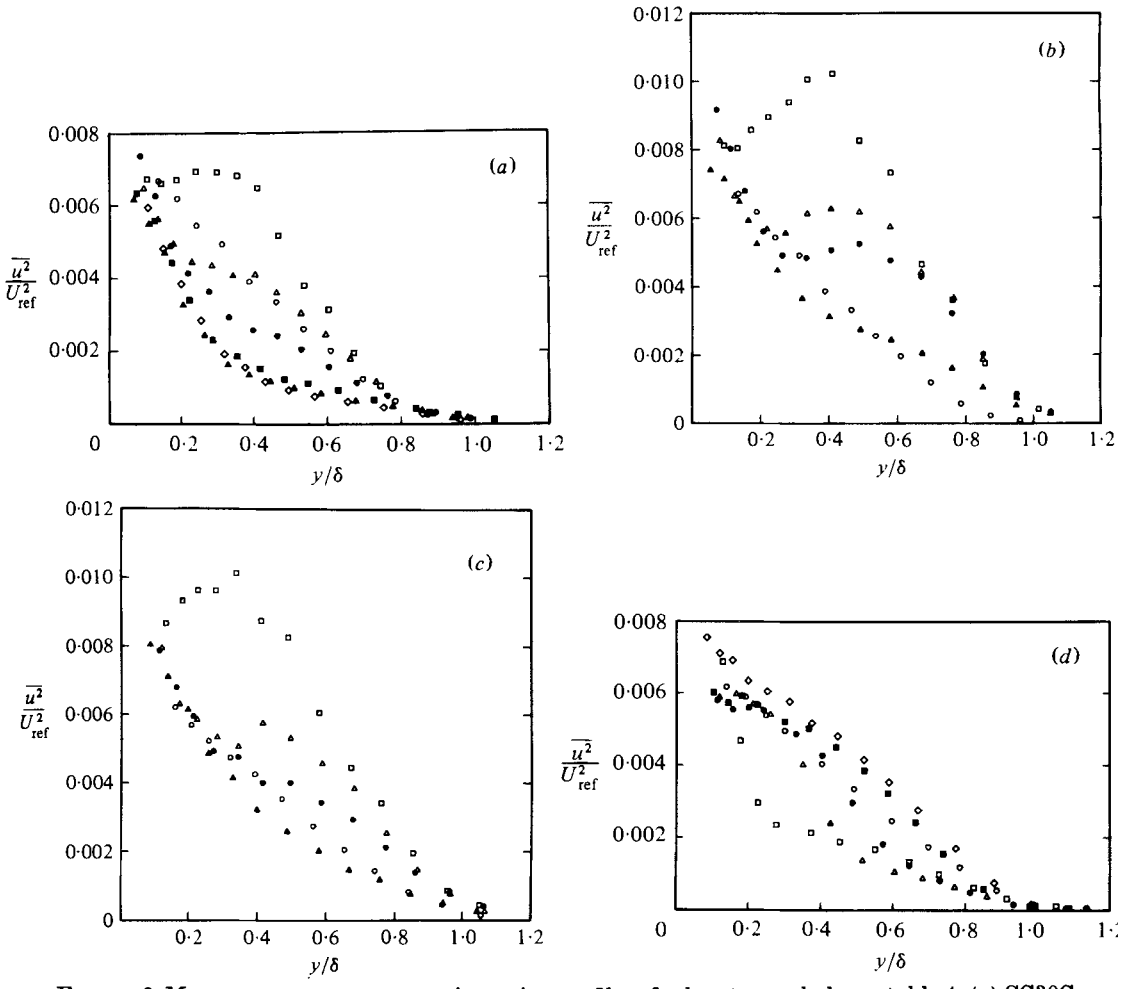

FIGURE 8. Mean-square u-component intensity profiles: for key to symbols see table 1. (*a*) CC30C; (*b*) CC30T; (*c*) CC20C; (*d*) CV30.

is needed before the detailed discussion (§ 5). As already stated, the effects of the longitudinal pressure gradient within the bend on the flow at exit are expected to be small, because the change of free-stream velocity from entry to exit is small, and are ignored below. Figure 2 gives the main points for the 30 degree bends.

3.2.1. *Initial response.* We begin by discussing changes within the bends; in figures 8–15 the profiles denoted by symbol ○ are at entry to the bends and those denoted by symbol □ are at exit (precise positions are given in table 1).

In all cases the largest effects of curvature are found in the outer layer, where the ratio of the extra strain rate $\partial V/\partial x$ to the simple shear $\partial U/\partial y$, or to a typical eddy strain rate, is largest. Close to the surface, the velocity and shear stress are connected by the law of the wall and, except in strong pressure gradients, neither will change drastically. Therefore the best entry to the results is to consider the effect of stabilizing or destabilizing curvature on shear-stress profiles whose end points, at $y = 0$ and $y = \delta$, are fixed or nearly fixed.

An increase in shear stress within the layer, as in the concave (CC) cases, leads to

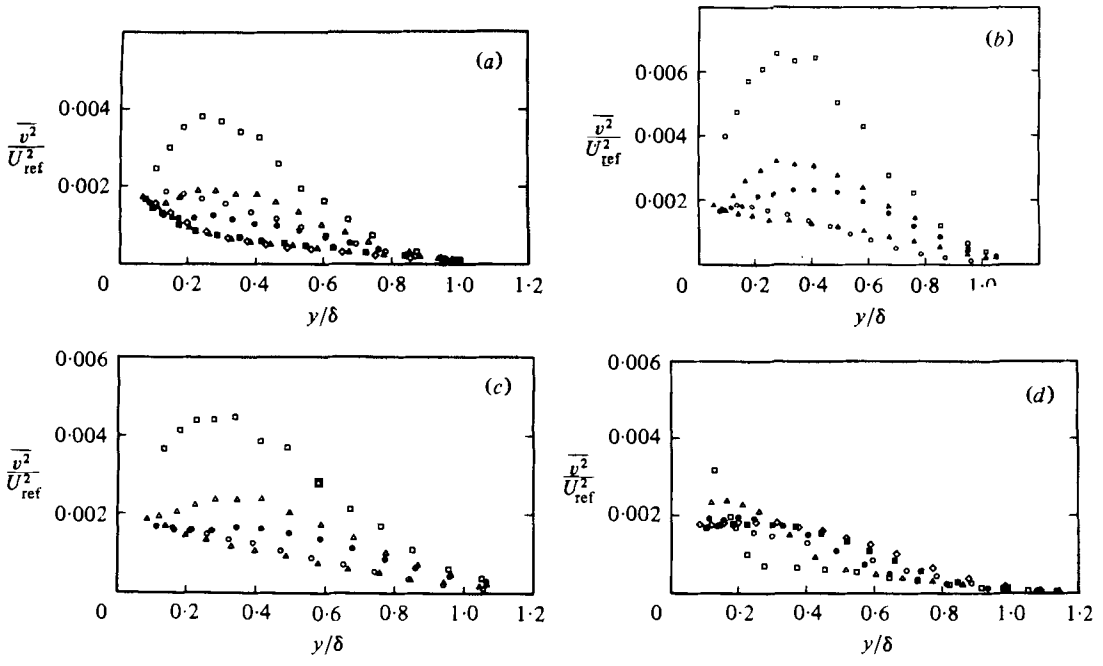

FIGURE 9. Mean-square v-component intensity profiles. (*a*) CC30C; (*b*) CC30T; (*c*)CC20T; (*d*) CV30.

positive $\partial(-\overline{uv})/\partial y$ near the surface and negative $\partial(-\overline{uv})/\partial y$ near the edge. It follows from the streamline-co-ordinate form of the momentum equation for a thin shear layer,

$$\frac{1}{\rho}\left(\frac{\partial P}{\partial x}\right)_{\psi} = \frac{\partial(-\overline{uv})}{\partial y}, \tag{1}$$

that the total pressure P increases along a streamline (ψ = constant) for values of y below the peak in $-\overline{uv}$, and decreases above the peak. In the case of CC30C it can be deduced from the mean velocity profiles (figure 7*a*) that the total-pressure change through the bend is an increase for $y/\delta < 0{\cdot}25$ and a decrease for $y/\delta > 0{\cdot}25$; the peak in shear stress (figure 10*a*) moves from $y/\delta = 0$ at entry to $y/\delta \simeq 0{\cdot}3$ at exit. The velocity gradient $\partial U/\partial y$ at $y/\delta \simeq 0{\cdot}25$ decreases by nearly a factor of three between entry and exit. In the convex case, CV30, the shear stress within the layer decreases, so $\partial(-\overline{uv})/\partial y$ at exit (figure 10*d*) is large and negative for $y/\delta < 0{\cdot}4$ and virtually zero for $y/\delta > 0{\cdot}4$. Therefore the total pressure decreases through the bend for $y/\delta < 0{\cdot}4$ and remains nearly constant for $y/\delta > 0{\cdot}4$; $\partial U/\partial y$ at $y/\delta \simeq 0{\cdot}1$ *increases* to nearly three times its value at entry. By the time the flow has reached the next measurement station (30 mm downstream of the bend exit proper) the resulting increase in the generation term $\overline{v^2}\,\partial U/\partial y$ in the shear-stress transport equation has led to the appearance of a sharp peak in shear stress at $y/\delta \simeq 0{\cdot}1$: this peak is therefore part of the recovery process rather than of the initial response to stabilizing curvature, which is, as just noted, a *decrease* in shear stress. It should be noted that the fact that $-\overline{uv}$ is close to zero for $y/\delta > 0{\cdot}4$ at the exit in CV30 is a coincidence; negative values of shear stress referred to co-ordinates aligned with the local surface are not prohibited.

The 'turbulent transport velocities' plotted in figure 14 and 15 also increase

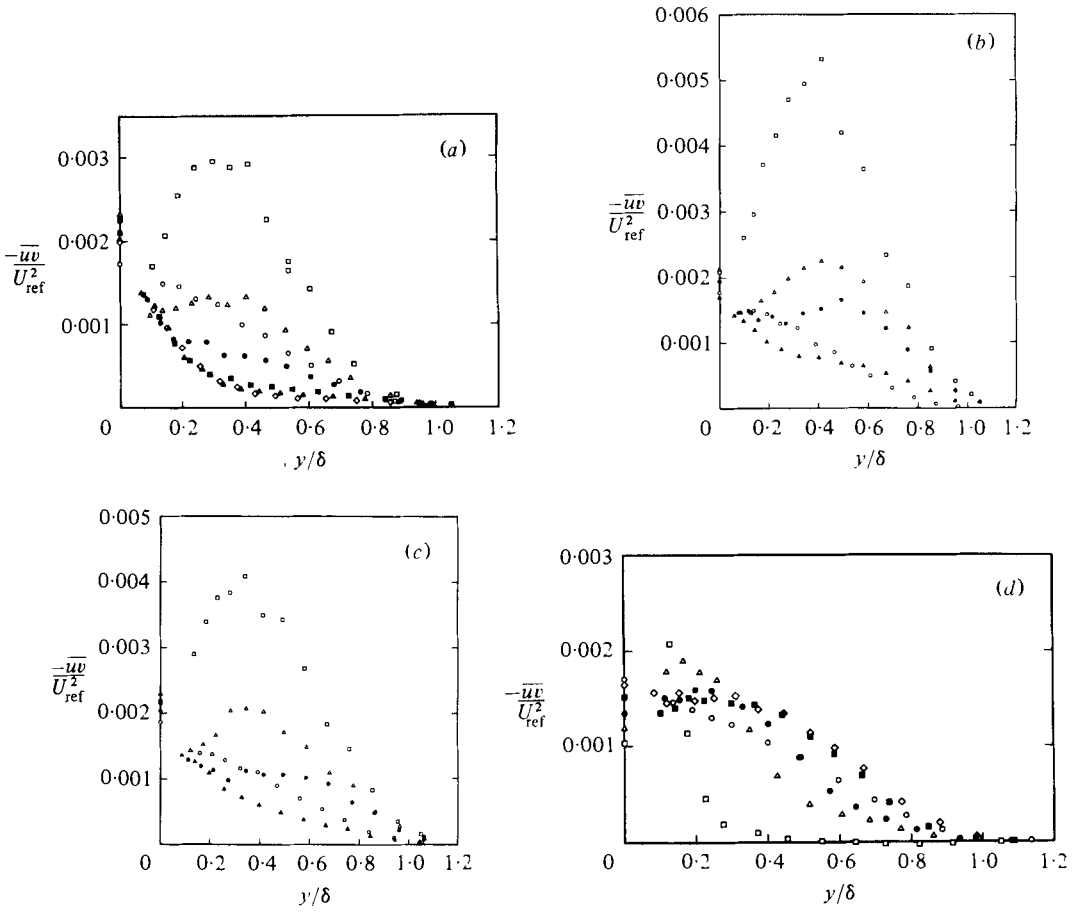

FIGURE 10. Shear stress profiles. (*a*) CC30C; (*b*) CC30T; (*c*) CC20C; (*d*) CV30.

markedly through the concave bends but have collapsed almost to zero at exit from the convex bend. The numerator of each transport velocity (e.g. $\overline{uv^2}$) is the triple-product group whose gradient with respect to y (e.g. $\partial\overline{uv^2}/\partial y$) is the turbulent transport term in the transport equation for the denominator (e.g. $\overline{uv}$). If turbulent transport were a pure convection by the large eddies, which is at least a good approximation to the facts, the transport velocities would be the ensemble-average V-component velocities of the large eddies. Normalized by the local mean velocity they would then give the tangents to the average large-eddy trajectories; in figures 14 and 15, U_{ref} is used for later convenience. The extremely small value of the turbulent energy transport velocity at exit in CV30 (figure 15*d*) suggests that the large eddy structure has been virtually destroyed by the convex curvature.

3.2.2. *Recovery*. The exit profiles in figures 8–15 (symbol □) represent the states of the turbulence very shortly after the regions of stabilizing or destabilizing curvature. The subsequent behaviour can be qualitatively explained from the interaction of the mean-velocity and shear-stress profiles (§ 4); a quantitative treatment must take account of the perturbations in the structure parameters and the transport velocities,

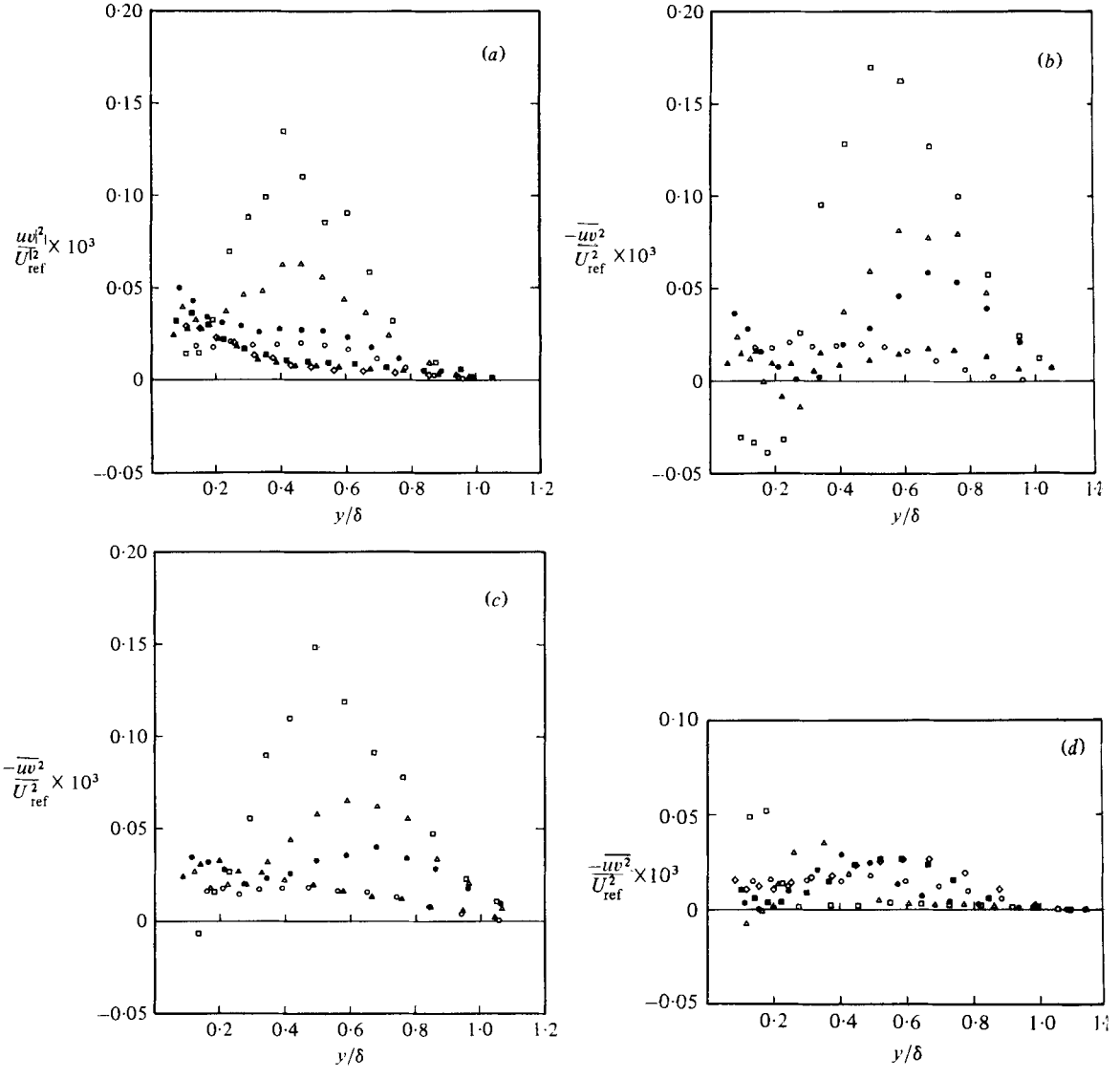

FIGURE 11. Profiles of $\overline{uv^2}$. (*a*) CC30C; (*b*) CC30T; (*c*) CC20C; (*d*) CV30.

but we postpone discussion of the structure, and of the large spanwise variations in the concave cases, until § 5.

Downstream of the convex bend, CV30, the turbulence intensity and shear-stress in the outer layer increase, and typical values of $\partial U/\partial y$ in the inner layer decrease, towards the self-preserving state. A combination of the high values of $\partial U/\partial y$ and of turbulent transport from below then causes turbulence quantities in the outer layer to rise above the self-preserving values. Figure 10*d*, in particular, shows the way in which the above-mentioned peak in shear stress near $y/\delta = 0{\cdot}1$ propagates outwards as a 'stress wave' (more properly a 'stress bore') and the turbulent transport velocities in figure 14 and 15 develop solitary waves related to this. The behaviour can be related to that of the curved mixing layer of Castro & Bradshaw (1976), in which collapse of

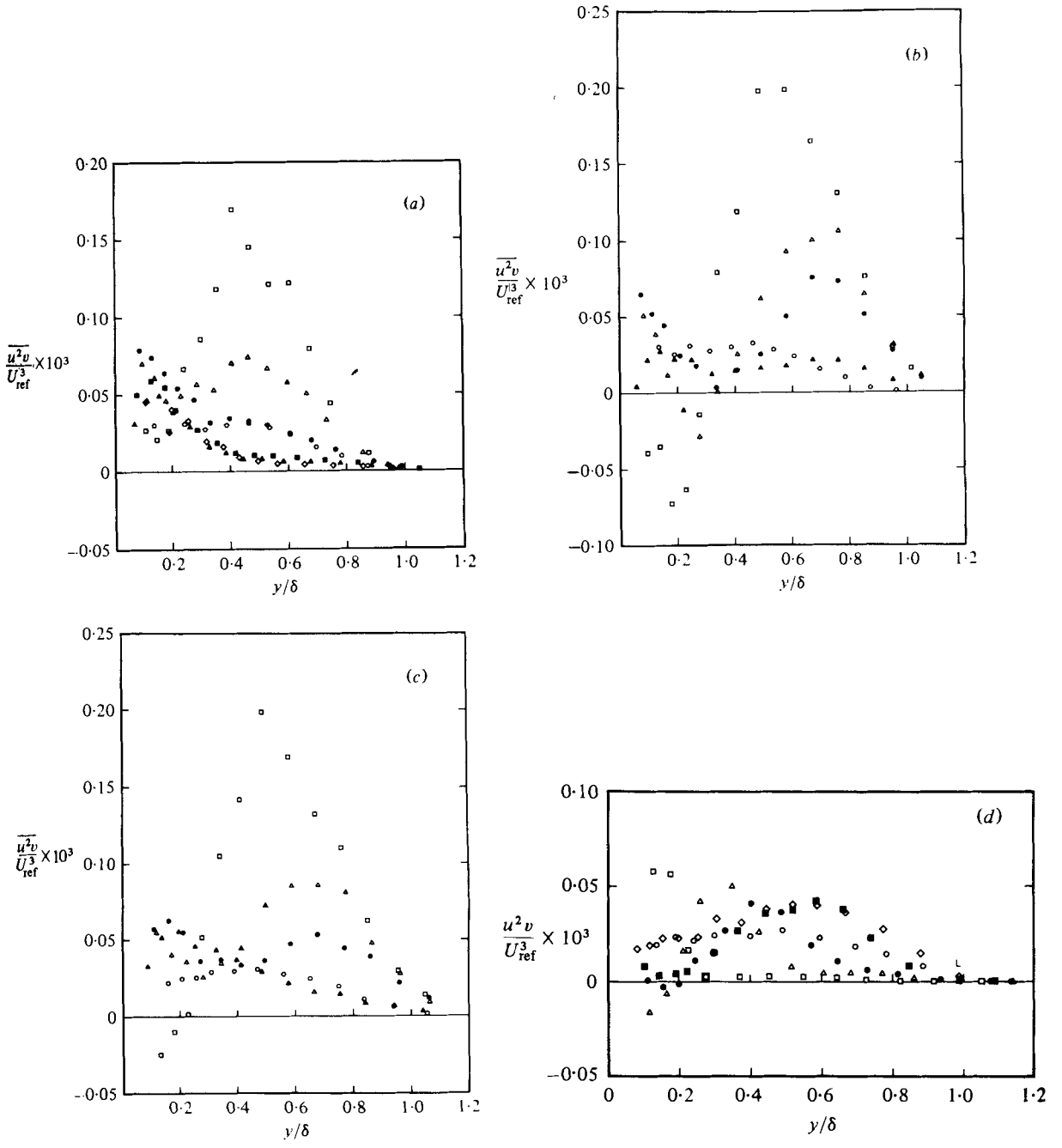

FIGURE 12. Profiles of $\overline{u^2v}$. (*a*) CC30C; (*b*) CC30T; (*c*) CC20C; (*d*) CV30.

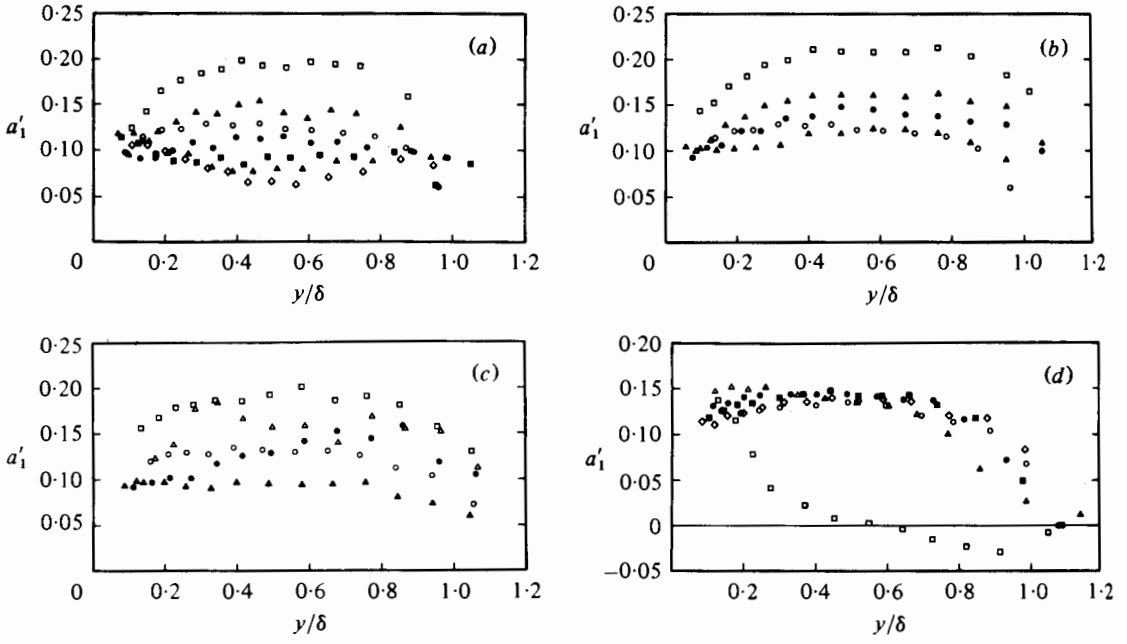

FIGURE 13. Profiles of shear-stress parameter $a_1' \equiv -\overline{uv}/1{\cdot}5(\overline{u^2}+\overline{v^2})$. (*a*) CC30C; (*b*) CC30T; (*c*) CC20C; (*d*) CV30.

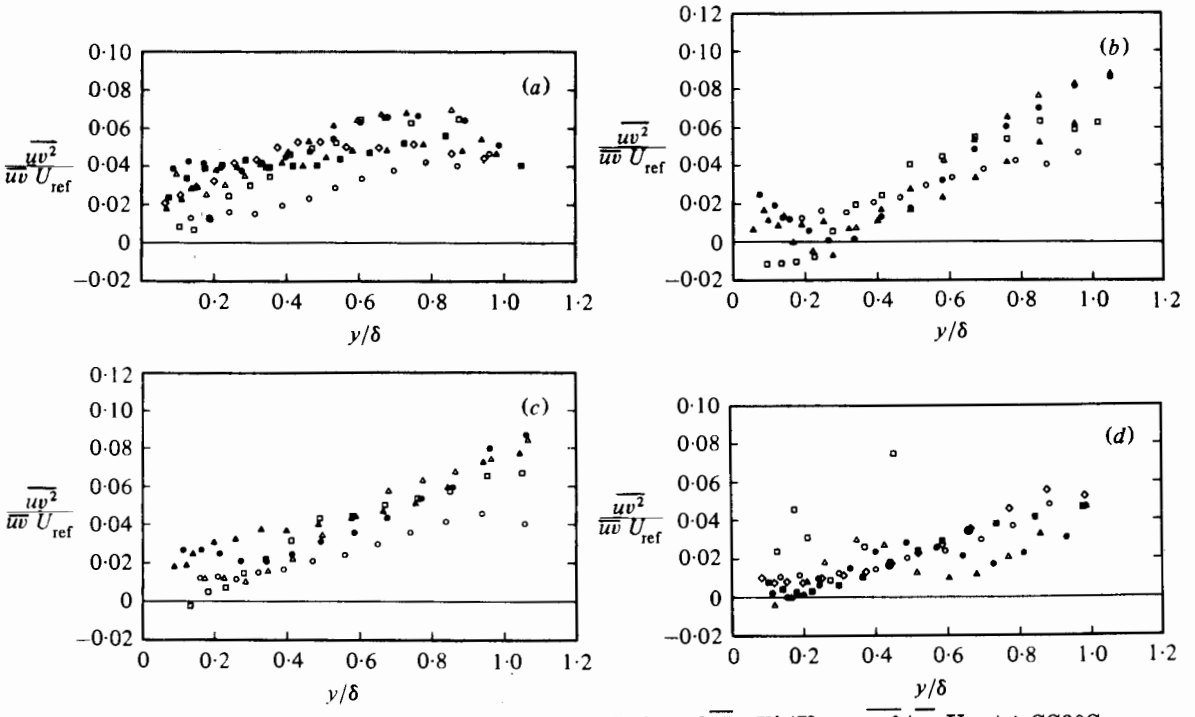

FIGURE 14. Profiles of turbulent transport velocity of $\overline{uv}$, $V_T'/U_{\text{ref}} \equiv \overline{uv^2}/\overline{uv}\,U_{\text{ref}}$. (*a*) CC30C; (*b*) CC30T; (*c*) CC20C; (*d*) CV30.

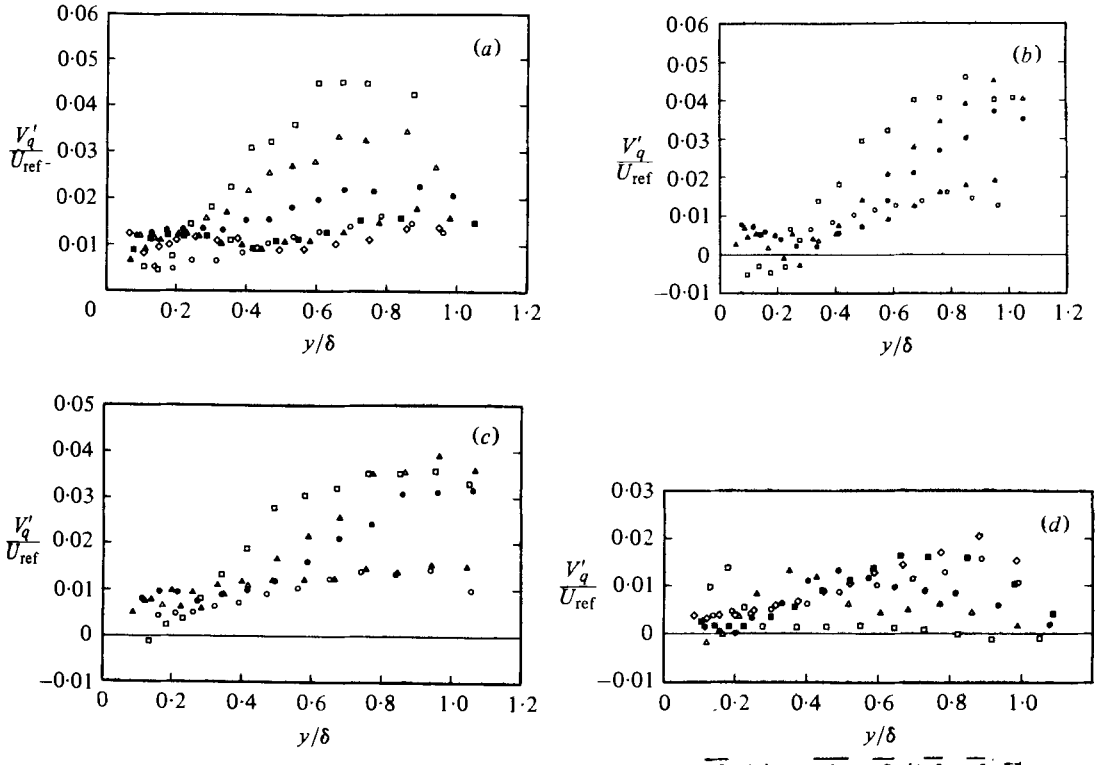

FIGURE 15. Profiles of turbulent transport velocity of $\overline{q^2}$, $V'_q \equiv (\overline{u^2v}+\overline{v^3})/(\overline{u^2}+\overline{v^2})\,U_{ref}$. (*a*) CC30C; (*b*) CC30T; (*c*) CC20C; (*d*) CV30.

the triple products (turbulent transport) leads to trapping of newly produced turbulence near the axis and thus to a rise above the self-preserving values. The 'stress bore' phenomenon did not appear in Castro & Bradshaw's flow; their measurements of profile peakiness (their figure 4 and p. 287) should have given some hint of it even if two stress bores, propagating in opposite y directions, appeared near the axis. However the rise above the self-preserving values did eventually extend to the whole profile, as in the present case.

Downstream of the concave bends the large shear stress gradients continue to reduce $\partial U/\partial y$ and H further below the self-preserving values. The minimum value of H in CC30C is 1·21 and the corresponding value of the Clauser parameter G is 4·04 compared with the self-preserving value of about 6·8. However the reduction in $\partial U/\partial y$ leads to a decrease in the rate of generation of all Reynolds stresses and a very rapid collapse of turbulent activity ensues. The details depend on the case considered; CC30C shows the largest effects. By $x = 183$ mm, $8\delta_0$ downstream of the exit, the shear stress in the rapidly responding inner layer has fallen below the upstream value (figure 10*a*) although the shear stress at the surface, and in the outer layer, is still well above the upstream value; thereafter, the surface shear stress continues to decrease, but only slowly, while the shear stress at $y/\delta = 0{\cdot}2$ (say) decreases with increasing x to barely half the upstream value, and the shear stress further out in the layer falls even more. It will be seen below that the 'eddy viscosity' $-\overline{uv}/(\partial U/\partial y)$, whether expressed as a dimensional quantity or normalized by $U_e\delta^*$ as usual,

remains well *above* the upstream value: thus the main reason for the collapse in Reynolds stress is the great decrease in $\partial U/\partial y$ (figure 7) brought about by the high shear-stress gradients in and just downstream of the bend. It is perhaps not surprising that the shear-stress parameter a_1' should fall below its usual value if $\partial U/\partial y$ is smaller than usual, but its decrease to barely half the upstream value (figure 13*a*) is remarkable.

The situation (large anisotropy and small mean shear) approximates the classical case of homogeneous turbulence emerging from a prolonged plane strain, and the rate of decay of anisotropy is comparable. For further analysis, see A.

It can hardly be doubted that the flow would in each case return to the self-preserving state if the test rig were long enough (and high enough to prevent the boundary layers meeting). However, the fact that the shear stress in the concave cases is so low, and still decreasing, at the last measurement station ($45\delta_0$ downstream of the bend exit in the case of CC30C) is a most spectacular consequence of *destabilizing* curvature!

4. Approximate analysis of impulse response

4.1. *Initial response*

Bradshaw (1973, 1974) argued that the time of response of the turbulence to a varying extra strain rate would be related to the conventional response time of about $3/(\partial U/\partial y)$ or, better, $3L/\tau^{\frac{1}{2}}$, where τ is the kinematic shear stress $-\overline{uv}$ and L is the dissipation length scale $\tau^{\frac{3}{2}}/\epsilon$; $3L/\tau^{\frac{1}{2}} \simeq 0{\cdot}5\overline{q^2}/\epsilon$, which is Townsend's dissipation time scale. If production and dissipation of turbulent energy are equal (local energy equilibrium) and $\overline{q^2} = 6\tau$, the two definitions of response time are the same. The final response of some structure parameter to the prolonged application of a constant, small extra rate of strain e can be plausibly expressed in a linearized and dimensionless form by an amplification factor $1 + \alpha_0 eL/\tau^{\frac{1}{2}}$, where $\tau^{\frac{1}{2}}/L$ is now being used as a typical r.m.s. eddy strain rate. The empirical 'constant' α_0 is of order 10 for several types of extra strain rate. Undoubtedly the response is not truly linear (e.g. Hoffmann & Bradshaw 1978); Koyama *et al.* (1978) have – in effect – derived values of α_0 as a function of $eL/\tau^{\frac{1}{2}}$ for the boundary layer on a surface rotating about a spanwise axis. However the weakest feature of the assumed amplification factor is its dependence only on the local rate of strain rather than on the rate-of-strain history. The response to a varying extra strain rate can be expressed, again in a plausible but unrigorous form, by replacing $\alpha_0 e$ by an 'effective' value E, governed by a simple first-order equation

$$U\frac{dE}{dx} = (\alpha_0 e - E)\frac{\tau^{\frac{1}{2}}}{L}. \tag{2}$$

Strictly the equation should be written in terms of the mean transport operator D/Dt, rather than as an ordinary differential equation, but this would be an unrealistic refinement in a linearized treatment that neglects turbulent transport. In the outer layer of a conventional boundary layer $UL/\tau^{\frac{1}{2}}$ is roughly 10δ.

Now from (2), the value of E at the end of a small strain impulse $\int e\,dt \equiv \theta$, where the integral is evaluated following the motion of the fluid and can be replaced approximately by $\int (e/U)\,dx$ or $\int e\,dx/U$, is given by

$$E = \frac{\alpha_0 \tau^{\frac{1}{2}}}{L}\theta. \tag{3}$$

The effective amplification factor $1+EL/\tau^{\frac{1}{2}}$ becomes $1+\alpha_0\theta$. In the case of streamline curvature, $e=\partial V/\partial x=-U/R$ (where R is strictly the radius of curvature of the *streamline*) so that θ as defined above is the turning angle, positive on a concave surface ($R<0$). Note that although $\int e\,dt$ is required to be small, e need not be. The analysis shows that the response of a structure parameter to a small rate-of-strain impulse is independent of position in the shear layer since y-dependent factors cancel. In practice a true impulse, with infinite e but finite θ, cannot be applied, and, especially near the surface where $L/\tau^{\frac{1}{2}}$ is small, the structure parameters will approach their equilibrium values in response to the finite rate of strain e. The above analysis is illustrated by the behaviour of $-\overline{uv}/\frac{1}{2}(\overline{u^2}+\overline{v^2})$ shown in figure 13; at exit from each bend this parameter is roughly constant across the boundary layer, except near the surface where the equilibrium effect of e is small. Of course θ is not small in the present experiments and this, plus the failure to apply a true impulse, means that quantitative predictions from the above linear analysis are not reliable. Rapid-distortion theory would cope with large turning angles but is valid, by definition, only over times that are short compared to the eddy response time (i.e. distances short compared with $UL/\tau^{\frac{1}{2}}$ or roughly 10δ).

It is remarkable that the equilibrium value of the amplification factor for the 30 degree concave bend, based on $\partial U/\partial y$ at the exit, is about $1+0{\cdot}3\alpha_0$ (say 4·0) at $y/\delta=0{\cdot}3$–$0{\cdot}4$, while the actual increase in shear stress at the exit is a factor between 2 and 5 depending on z. The amplification factor relates to structural parameters rather than dimensional, derived quantities like shear stress, but it is evident that the response to large rates of strain is certainly not much smaller than that predicted by the linear formulae developed for small rates of strain. That is, nonlinearities do not seriously limit the response even when the destabilizing extra strain rate is large as in the present case.

4.2. *Recovery*

We discuss the recovery of the boundary layer, after the extra strain rate has fallen to zero, in terms of a crude Reynolds-stress-transport model that gives simple analytic results. Consider constant pressure flow and write the mean-motion equation and the Reynolds shear-stress transport equation in two dimensions as

$$\frac{DU}{Dt}=\frac{\partial\tau}{\partial y}, \tag{4}$$

$$\frac{D\tau}{Dt}=v^2\frac{\partial U}{\partial y}-\overline{p'\left(\frac{\partial u}{\partial y}+\frac{dv}{\partial x}\right)}+\ldots. \tag{5}$$

Differentiating (4) with respect to y gives, using the two-dimensional continuity equation but without further approximation,

$$\frac{D}{Dt}\left(\frac{\partial U}{\partial y}\right)=\frac{\partial^2\tau}{\partial y^2}. \tag{6}$$

Writing X for the perturbation in $\partial U/\partial y$ from its initial value, and making some plausible approximations in (6) typical of those used in turbulence models (see A for details), it can be shown that

$$\frac{D^2X}{Dt^2}+1{\cdot}5\frac{\tau^{\frac{1}{2}}}{\delta}\frac{DX}{Dt}+2{\cdot}5\frac{\tau}{\delta^2}X=0, \tag{7}$$

where the values of the coefficients are rough estimates. This equation represents damped simple harmonic motion with a time period (following the motion of the fluid) of about $4\delta/\tau^{\frac{1}{2}}$ and damping of about half the critical value.

The result that the response of a turbulent shear layer to a perturbation is a damped oscillatory variation in $\partial U/\partial y$ (and τ) would still hold if the coefficient of DX/Dt was up to twice the estimated value or if the coefficient of X were up to *four* times smaller. It can be deduced from equation (6) that the shear-stress perturbation varies in quadrature with the perturbation in velocity gradient. In practice the response is nonlinear; the period will be closer to the *local* value of $4\delta/\tau^{\frac{1}{2}}$ than to the initial value, and the present results show that if τ falls to a low level the period of oscillation becomes very long. However the above demonstration that oscillatory response can occur, even when the choice of structural parameters is appropriate to a mildly perturbed layer, is useful; in particular it warns us not to attribute the oscillatory response of the present flow solely to large structural changes caused by curvature.

5. Discussion

The general behaviour of the mean velocity and shear-stress profiles has been qualitatively explained in § 3, with some quantitative but empirical analysis in § 4. We now discuss the detailed behaviour of the mean velocity, Reynolds stresses and triple products, with emphasis on the changes in those dimensionless structure parameters that are effectively constant in conventional boundary layers.

5.1. *The mean velocity profiles and* c_f

The mean profiles are plotted on semi-logarithmic scales in figures 7(*a*)–(*d*). The values of the friction velocity $u_\tau \equiv U_e\sqrt{(\frac{1}{2}c_f)}$ used in figure 7 were chosen, by a computer routine, to optimize the fit to the logarithmic law of the wall close to the surface. The additive constant in the logarithmic law was chosen as 5·2, rather than the usual value of 5·0 (Coles & Hirst 1969, p. 5): several sets of measurements in undisturbed wall shear layers at Imperial College (see, e.g., Brederode & Bradshaw 1978) show that this value gives the best agreement with Preston-tube measurements of surface stress, using the calibration of Patel (1965) which appears to be of very good accuracy. The profile for CV30 at $x = 30$ mm (figure 7*h*) has defeated the computer routine and the dotted line, for which u_τ is reduced by a factor of 0·88, is a more plausible fit. Elsewhere, the region of logarithmic fit is extensive enough to give fair confidence in the value of u_τ: recall that the effects of extra mean strain rates decrease near the wall because the r.m.s. eddy strain rate increases, and that at the profile measurement stations the pressure gradient is small enough to have no effect on the viscous sublayer or the additive constant in the logarithmic law.

The development of the dip below the logarithmic mean-velocity profile within the concave bend is shown in detail in II, but merits a qualitative explanation at this point. The effect of destabilizing curvature is to increase the dissipation length scale L (normally $0{\cdot}41y$) by an amount that increases with distance from the wall. Thus the mean velocity gradient predicted from the local-equilibrium formula,

$$\text{production} \equiv \frac{\tau\,\partial U}{\partial y} = \text{dissipation} \equiv \frac{\tau^{\frac{3}{2}}}{L}, \tag{8}$$

tends to decrease below the standard value, $u_\tau/(0{\cdot}41y)$; evidently this tendency overwhelms the increase in $\partial U/\partial y$ caused by an increase in shear stress. Similar effects of unusually large length scales are found in reattachment regions (Bradshaw & Wong 1972; Chandrsuda 1976). In the present measurements for CC30 the dip is still pronounced at $x = 335$ mm, about $15\delta_0$ from the exit, but has vanished – though the profile shape is still odd – by $x = 635$ mm ($29\delta_0$). The behaviour in CC30T is similar. In CC20 the dip has just disappeared at $x = 310$ mm. In CV30 the departure from the logarithmic law again occurs close to the surface but, being in the usual sense, is less spectacular. The conventional 'wall-plus-wake' profile families would clearly produce poor fits, especially to the CC profiles.

5.2. *The shear-stress profile*

The shear stress and the normal stresses are linked via the generation terms in their transport equations; it is simplest to discuss the shear stress first, and then consider the structural parameters defined as ratios of shear stress to various combinations of normal stresses. The general features of the shear-stress response, large increase or decreases within the concave or convex bends followed by a return to equilibrium which is non-monotonic in each case, have been discussed above. Here we concentrate on the return to equilibrium.

The most remarkable feature of the shear stress profiles for the concave bends at the spanwise position of maximum c_f (the 'crest') is the persistence of the low values in the outer layer. In CC30C the last three profiles, covering a distance of over 600 mm or 30 times the entry boundary-layer thickness δ_0, are virtually identical when plotted against y/δ (or against y itself, since δ increases by only about 20 per cent between these stations). The less extensive measurements for CC20C suggests that the behaviour there is similar. In CC30T, the shear stress in the outermost part of the layer remains above the initial value and the general level is much higher than at the crest position. This is partly the result of the higher values of shear stress at exit, but the differences in profile *shape* at $x \simeq 900$ in figures 10(a) and 10(b) (solid triangles) are in the sense which would be produced by transport towards the wall at the crest position and transport away from the wall at the trough. Transport in these senses can be provided by longitudinal vortices whose axes lie midway between the peak and trough positions, and whose diameter is somewhat less than the layer thickness so that the V component velocities at $y/\delta \simeq 0{\cdot}5$ are *larger* than near $y/\delta = 1$. Figure 6(h) shows the spanwise variation of the tranverse shear stress, $-\overline{uw}$, for CC30 at $x = 945$ mm, $y/\delta \simeq 0{\cdot}09$. Comparison with the spanwise variation of u component mean velocity, figure 6(e), shows that $-\overline{uw}$ is roughly proportional to $\partial U/\partial z$: the maximum value of $|\partial\overline{uw}/\partial z|$ is only about 15 per cent of the local value of $|\partial\overline{uv}/\partial y|$, so that, as might be expected from the persistence of spanwise variations in general, the transverse transport of momentum does not have a large effect on the U component of mean velocity. Clearly $\overline{uw}$ opposes the transport of momentum by the W component associated with the hypothetical longitudinal vortices. A final summary of the evidence for longitudinal vortices is given in § 5·5.

On the convex side of the duct, the most noticeable feature of the recovery is the 'stress bore' which will be discussed in connexion with the triple products in § 5.4 below. The overshoot of the shear stress in the outer layer above the upstream values is pronounced, although c_f remains below the constant-pressure value. The results

are a useful example of the way in which a turbulent region will grow to fill the whole of a region of mean shear.

5.3. *The intensity profiles*

The profiles of $\overline{u^2}$ and $\overline{v^2}$ ($\overline{w^2}$ was not measured in the present experiment) follow the same general trend as $-\overline{uv}$ but less strongly. The sum $\overline{u^2}+\overline{v^2}$ is invariant with respect to rotation of the axes so that the change that occurs round the bend can be attributed wholly to streamline curvature effects: it is too large to be explained entirely by the change in turbulent energy production $-\overline{uv}\,\partial U/\partial y$ and therefore corresponds to a change, of opposite sign, in the dissipation rate. The behaviour of the terms in the transport equations for turbulent energy and shear stress will be discussed below; the simplest way to discuss the intensity measurements themselves is to consider the dimensionless parameters $a_1' \equiv -\overline{uv}/[\frac{1}{2}(\overline{u^2}+\overline{v^2})] \simeq -\overline{uv}/(\overline{u^2}+\overline{v^2}+\overline{w^2})$, or $\overline{v^2}/\overline{u^2}$. Townsend (1976, p. 107) tabulates values of the various stress ratios in undistorted shear layers.

On the concave side of the 30 degree bend, a_1' (figure 13*a*) increases from the upstream value of about 0·13 over most of the layer to a maximum value of about 0·20 at exit from the bend, slightly more for CC30T than for CC30C. This maximum value is attained only for $y/\delta > 0{\cdot}4$; for $y/\delta < 0{\cdot}1$, where curvature effects are small, a_1' remains near the upstream value. Further downstream of the exit, a_1' decreases with increasing x, the profile developing a dip in mid-layer; the values for CC30C are still falling at the end of the test section where the minimum value on the profile, at $y/\delta \simeq 0{\cdot}5$, is about 0·065, half the upstream value and a third of the maximum. In CC30T, a_1' has returned to the upstream value by the end of the test section, but appears to be still decreasing. In CC20, the behaviour is a less violent form of that in CC30; the maximum value of a_1' is about 0·19 and the value at the last station, again still decreasing with x but in this case varying little with y, is nearly 0·10. These results show that in the region of 'recovery' from the effects of the bend the efficiency of maintenance of shear stress, represented by a_1', decreases; the decrease is not as marked as in the shear stress itself because the intensities also decrease, but the structural changes are large, particularly at the 'crest'. Abnormally low values of the shear-stress correlation coefficient $-\overline{uv}/(\overline{u^2}.\overline{v^2})^{\frac{1}{2}}$ were found by So & Mellor (1975) in their prolonged concave bend, and attributed by them to the effects of longitudinal vortices: however the low values occurred at the *trough* while in the present case they occur at the *crest*.

At exit in CV30, a_1' falls significantly below zero in the outer half of the layer: the actual values are the ratios of small measured quantities and should not be taken as accurate in detail. At the next profile downstream, 6 boundary-layer thicknesses later, a_1' has practically recovered to its upstream value for $y/\delta < 0{\cdot}8$, and recovery in the outer 20 per cent of the flow follows soon after. The shear stress and intensities, it will be recalled, actually overshoot the upstream values but this can be explained without invoking structural changes. Indeed, because the stabilizing effects are so large, the turbulence is almost obliterated in the bend and the newly created turbulence does not experience any curvature effects on its structure except through faint memories of the behaviour in the bend.

The shear correlation coefficient, and the ratio $-\overline{uv}/\overline{u^2}$, tend to follow the behaviour

of a_1': the maximum value of the shear correlation coefficient, at exit from the bend in CC30T, is 0·64 compared to an upstream value of about 0·43.

It seems likely intuitively that the main effect of the stabilizing or destabilizing 'centrifugal' body forces produced by the curvature will be on the v (radial) component, and the ratio $\overline{v^2}/\overline{u^2}$ is therefore of some interest. Values are not plotted here because the main trends can be easily summarized. At $y/\delta \simeq 0{\cdot}5$ the upstream value of $\overline{v^2}/\overline{u^2}$ is about 0·4. In CC30C it rises to 0·57 at exit and then falls back to about 0·5 by the next station: taken at face value the data show a fall to 0·47 at $x = 335$ and then a rise to 0·54 at the end of the test section, but it is difficult to believe that there are really two maxima. In CC20C $\overline{v^2}/\overline{u^2}$ rises to 0·5 at exit and then falls back to about 0·42 with no further consistent trend within the test section. In CC30T, $\overline{v^2}/\overline{u^2}$ at $y/\delta \simeq 0{\cdot}5$ falls to 0·35 at exit and continues falling to a near-constant value of only 0·25. In CV30, $\overline{v^2}/\overline{u^2}$ at $y/\delta \simeq 0{\cdot}5$ remains near 0·4 except that the measured value at $x = 183$ is 0·5; this is the point at which the outgoing 'bore' of newly created turbulence has reached $y/\delta \simeq 0{\cdot}5$, and evidently small structural changes occur near the bore.

The inner-layer values of $\overline{v^2}/\overline{u^2}$, like the values of a_1', are little affected by curvature. In summary, $\overline{v^2}/\overline{u^2}$ rises, as expected, at the end of the concave bends, but thereafter the behaviour is almost the opposite of the behaviour of a_1', *high* values persisting at $c_{f,\max}$ and *low* values soon appearing at $c_{f,\min}$. The convex-side behaviour is unremarkable.

5.4. *The triple products*

Triple products of velocity fluctuations appear in the turbulent-transport terms of the transport equations for turbulent energy and shear stress, and seem to be determined mainly by the large eddies. They are likely to be strongly affected by curvature, but few measurements have been made in curved flows. The measurements of Ramaprian & Shivaprasad (1978) were made with unlinearized (constant-current) hot wires and appear to be seriously in error; their values of $\overline{u^2 v}/u_\tau^3$ on a flat surface are smaller than our values at entry by a factor of about 1·7 (1·5 in the case of $\overline{v^3}$).

The triple products are most conveniently presented and discussed in the form of y component turbulent transport velocities for shear stress and turbulent energy, defined respectively as

$$V_\tau = \overline{uv^2}/\overline{uv} \tag{9}$$

and

$$V_q = \overline{q^2 v}/\overline{q^2} \simeq \frac{\overline{u^2 v} + \overline{v^2}}{\overline{u^2} + \overline{v^2}}, \tag{10}$$

where $\overline{q^2} = u^2 + v^2 + w^2$ and the last element of (10) is the approximation measured in the present experiment. The results are presented as V_τ/U_{ref} and V_q/U_{ref}, which are not true turbulence parameters; strictly, V_τ and V_q should be normalized by a typical velocity scale of the outer-layer turbulence, say $[\int(-\overline{uv})\,dy/\delta]^{\frac{1}{2}}$, where the integral is over the outer layer only, but the choice of such a scale would be controversial and confusing. The neglect of pressure transport is also controversial and is discussed in A.

If the transport equation for a Reynolds stress reduces to 'mean transport = turbulent transport' at the edge of the boundary layer, which is true for turbulent

energy ('advection' = 'diffusion') but not for shear stress, then the turbulent transport velocity at the edge is equal and opposite to the entrainment velocity. In this case, normalization by U_e gives an immediately recognizable quantity; V_q/U_e is equal to $d(\delta-\delta^*)/dx$ in a constant-pressure, two-dimensional boundary layer. In undisturbed boundary layers, V_τ and V_q rise roughly linearly from the surface to plateau values at the edge of the flow. At the Reynolds number of the present tests, the plateau values for V_τ/U_e and V_q/U_e are respectively 0·04 and 0·016.

At exit from the bend in CC30C, V_τ has almost doubled and V_q almost trebled, except in the outer third of the boundary layer where the exit values reach plateaux while the upstream values are still increasing with y (the absolute values of triple products increase by factor of six or more in mid-layer; recall that these increases occur over a streamwise distance of about seven boundary-layer thicknesses). It is noteworthy that the transport velocities remain positive although the intensity and shear-stress profiles have pronounced peaks at $y/\delta \sim 0{\cdot}3$–$0{\cdot}4$; a 'gradient diffusion' model of turbulent transport would give the wrong sign for the triple products in the inner third of the boundary layer, probably leading to prediction of large changes in the inner layer which do not in fact occur. In conventional boundary layers where shear-stress peaks result from prolonged pressure gradient, turbulent transport in the inner layer *is* towards the surface, as is well shown by recent measurements in nearly self-preserving boundary layers at R.A.E., Bedford (L. F. East, private communication). Further downstream on the line of $c_{f,\max}$ the transport velocities in the outer layer decrease again, V_q at once but V_τ only for $x > 335$. At the last station, V_q in the outer layer has fallen slightly but significantly below the initial value while V_τ is somewhat above it. Inner-layer values of both transport velocities increase to maximum values as large as the outer-layer plateau values in the undisturbed boundary layer by $x > 335$, and then decrease slowly; this reflects the appearance of large negative gradients of shear stress and intensity in the inner layer, and implies quite large changes in inner-layer structure not apparent from the second-order parameters like a_1'.

In CC30T the behaviour is similar to that at $c_{f,\max}$ except that V_τ and V_q go negative in the inner layer at the exit station only (the positive slopes of the shear stress and intensity profiles being even larger here than on the line of $c_{f,\max}$). The subsequent rise in inner-layer values is also smaller (the intensity profiles at $c_{f,\min}$ do not develop the large negative gradients in the inner layer found at $c_{f,\max}$). As usual, the behaviour in CC20C is similar to that in the CC30 cases but less pronounced.

In CV30, V_q at exit is almost exactly zero for $y/\delta > 0{\cdot}3$, while in the inner layer a peak, nearly as large as the plateau value in the upstream boundary layer, appears. Subsequently the peak propagates outwards, although even outside the peak the V_q values start to recover. The peak in V_q occurs at about the position of maximum negative $\partial(\overline{u^2}+\overline{v^2})/\partial y$. At the end of the test section, V_q slightly exceeds the upstream values in the outer half of the layer. At exit from the convex bend V_τ goes to infinity at $y/\delta \simeq 0{\cdot}6$, where $-\overline{uv}$ passes through zero. As in V_q, a peak appears near $y/\delta = 0{\cdot}2$ and propagates outward in step with the negative peak in $\partial(-\overline{uv})/\partial y$. The recovery of V_τ and V_q in the convex bend is much slower that that of a_1', but keeps pace with the recovery of the shear stress and intensity. The general behaviour of the transport velocities is consistent with the expected dominance of turbulent transport by the large eddies. Since the large eddies contain (as well as transporting) most of the energy and shear stress we expect their reaction time to be of the same order as that of the

energy. Alternatively, one might argue that since the response to a perturbation cannot be complete until large eddies have had time to migrate across the shear layer, the reaction time should be of order δ/V_τ at least; however, as shown in A, the speed of propagation of a disturbance exceeds the transport velocity itself.

The triple products themselves are determined by transport equations which have turbulent-transport terms of their own. To the thin-shear-layer approximation, the turbulent transport term in the $\overline{uv^2}$ equation is $\partial(\overline{2p'uv}/\rho + \overline{uv^3})/\partial y$ so that the contribution of the quadruple velocity product leads to a 'transport velocity' $\overline{uv^3}/\overline{uv^2}$. Measurements for CC30C (see A) show that the behaviour of the transport velocity of $\overline{uv^2}$ in CC30C is nothing like that of the transport velocities of $\overline{uv}$ and $\overline{q^2}$: in the inner layer, it reaches a value of nearly $0{\cdot}5U_{\text{ref}}$, not much less than the local mean velocity, while in the outer layer it falls towards zero with no indication of asymptoting to a value of order $U_e\,d\delta/dx$ as V_τ does. Downstream of the bend in CC30C, the transport velocity of $\overline{uv^2}$ follows very roughly the same trend as the shear stress, large values at exit being followed by a rapid decrease further downstream; results for the other cases also tend to follow the trend of shear stress. While the accuracy of the results may not be high they undoubtedly demolish the hypothesis of roughly equal transport velocities for all quantities transported by the large eddies. However, the transport velocity of $\overline{uv^2}$ is better behaved than its eddy diffusivity; the profiles of $\overline{uv^2}$ just downstream of the bend in CC30C have marked peaks near $y/\delta = 0{\cdot}4$, but the turbulent transport of $\overline{uv^2}$ is everywhere outwards (i.e. $\overline{uv^3}$ is positive).

As shown in A, the 'bore' of turbulent intensity that propagates outward from the inner layer downstream of the convex bend is the joint result of turbulent transport *and* of interaction between the turbulence and the mean flow.

5.5. *Longitudinal vortices*

As in the case of most other experiments in curved flows, the results are consistent with the presence of nearly steady contra-rotating longitudinal vortices in and downstream of the concave bends. The spanwise variations are so large that the amplitude of any spanwise wandering of the vortex positions must be a small fraction of δ. Johnston *et al.* (1973) found significant wandering and intermittency of the vortices in a rotating duct flow, especially for weak rotation corresponding to curvature with δ/R of order $0{\cdot}01$. However, the essential difference between a boundary layer and a fully developed duct flow is that, by definition, the latter is independent of entry conditions whereas a growing boundary layer in a wind tunnel continues to entrain weak longitudinal vorticity created by the damping screens: it therefore acquires spanwise variations, even on a plane surface, and these evidently determine the distribution of the much stronger longitudinal vorticity that arises via the Taylor–Görtler inviscid instability mechanism. Since the disturbances caused by the screens have an irregular waveform (large range of spanwise wavelengths) the curvature-induced vortices can select an average wavelength related to the boundary-layer thickness although, as the present results (e.g. figure 6) show, the vortex 'crest' positions usually correspond to some of the maxima in the upstream c_f pattern. Preliminary measurements in the present work certainly showed that the position, and to some extent the amplitude, of spanwise variations of skin friction and other properties depended on the wind-tunnel screens. It should be noted that on aircraft,

or in turbomachines, spanwise variations will be introduced by variations in transition position, which is extremely sensitive to surface imperfections; therefore the vortices formed on concave surfaces will probably be fairly steady as in the present case. The upstream boundary layer in So & Mellor's experiment was more uniform than ours, but their vortex pattern appeared to be steady and very strong, although, curiously, they report negligible spanwise variations in skin friction despite variations of more than 10 per cent in the mean velocity in the inner layer. The measurements of Ellis & Joubert (1974) in curved ducts of aspect ratio about 13:1 showed spanwise variations in the case of the 75 in. radius duct but not in the 15 in. radius duct, the variations in the former case being unaffected by entry disturbances. Evidently a vortex system which is steady enough to affect the mean velocity *can* occur in a curved duct, but may not always do so.

So & Mellor (1972, 1975) discuss the vortex pattern in some detail. Their original suggestion (1972) that two co-rotating vortices, one above the other, occur at a given spanwise position is not reasonable; internal shear layers would form between such vortices and almost certainly lead to their amalgamation. So & Mellor also produce evidence that the vortex pattern weakens at large distances downstream from the start of curvature even though δ/R remains large. This is likely to be a transient effect, caused by the decrease in the ratio of vortex wavelength to boundary-layer thickness δ as δ grows; vortices of diameter much less than the shear-layer thickness are likely to be destroyed by turbulent mixing and the above-mentioned bias against co-rotating vortices implies that *pairs* of vortices will disappear. Even in a test rig of infinite width, the disappearance of one pair is likely to trigger the disappearance of another pair two or more wavelengths away, and so on, so that the average wavelength may increase in fairly sudden jumps of a factor of two (say) every time δ has doubled (say) rather than increasing more slowly due to sporadic disappearances. Clearly, the strength of the vortices would be affected by wavelength changes, but on a surface of constant δ/R the long-term average strength should remain constant. In test rigs of finite width, side-wall constraints are likely to affect vortex behaviour, as is notoriously the case for flow between rotating cylinders: in the present work the test-rig width was 35 times the boundary-layer thickness at entry, δ_0, so that 17 or 18 vortex pairs, each with diameter δ_0, say, could be accommodated. At the end of CC30, the ratio of boundary-layer thickness to rig width was roughly $\frac{1}{14}$, about the same as in So & Mellor's concave-wall flow. Meroney & Bradshaw (1975; see also Hoffmann & Bradshaw 1978) with the same entry conditions as the present work but $\delta/R \simeq 0{\cdot}01$–$0{\cdot}02$, found spanwise variation of c_f suggesting longitudinal vortices but Ramaprian & Shivaprasad (1978), again with $\delta/R \simeq 0{\cdot}01$–$0{\cdot}02$ but with a ratio of boundary layer thickness to rig width of as much as $\frac{1}{6}$, found no evidence of the presence of vortices. So & Mellor suggest that the weakening of the vortices in their flow caused an increase in turbulent intensity; if this is a general result the causative connexion may not be direct. It is noteworthy that the ratio of the boundary-layer thickness at the trough to that at the peak was almost 2:1 in So & Mellor's flow but never exceeded 1·3:1 in CC30: the prolonged curvature in So & Mellor's flow evidently produced very strong vortices indeed.

The explicit evidence for the presence of vortices is shown in figure 6. Figure 6(*d*) shows the remarkable persistence of the c_f pattern downstream of the 30 degree concave bend, and figure 6(*e*) shows a similar persistence in the lateral variation of

mean velocity U at $y/\delta \simeq \frac{1}{4}$. Figure 6(*g*) shows that the patterns for the three measured Reynolds stresses at $y/\delta \simeq \frac{1}{4}$ are very similar to each other and a reasonably exact *inverse* of the patterns for c_f or U. The triple-product patterns in figure 6(*h*) are close to each other and to the c_f pattern: the ratio of 'crest' to 'trough' values at $y/\delta \simeq \frac{1}{4}$ is as much as 5:1. An explanation for these results is that negative values of $V-\overline{V}$ due to vortex motion near the 'crest' (figure 6*f*) lead to the inward transfer of fluid with high mean velocity and low Reynolds stress; the logarithmic law ensures that high surface shear stress goes with high mean velocity, and the result is large negative gradients of Reynolds stress near the surface leading to large outward transport by triple products. Near the 'trough' the opposite effect occurs.

The V measurements at $x = 1443$ mm (figure 6*f*) show a very similar pattern to c_f: however, the measurements at $x = 168$ do not correspond very closely to c_f. In other respects the vortices appear to be fully formed at the bend exit, but it must be remembered that V and W are quite small: estimating the vortex diameter as 20 mm and the circumferential velocity as $0{\cdot}05U_e$, the distance for the vortex to complete one revolution is about 1200 mm, the same order as the downstream length of the test rig.

The large spanwise variation of mean quantities described above are strong evidence for the presence of *mean* longitudinal vortices and the work of Johnston *et al.*(1973) suggests that the eddy structure consists mainly of (fluctuating) longitudinal vortices also. The fluctuating longitudinal vortices will decay in plane flow, and will eventually be replaced by the 'mixing jet' large-eddy structure (Grant 1958: Brown & Thomas 1977), typical of plane flows, whose predominant vorticity is spanwise. Now it seems very likely that the intermediate stage, in which the large eddies are a mixture of longitudinal vortices and mixing jets interacting with each other, will be a rather inefficient producer of shear stress; put another way, the presence of two competing large-eddy systems is unlikely to lead to higher efficiency than an undisturbed monopoly. This would explain the reduction in a_1'. The general differences between properties on the lines of $c_{f,\max}$ and $c_{f,\min}$ – most notably the fact that $\overline{v^2}/\overline{u^2}$ is only half as large on the latter line as on the former – suggest that the downstream effect of the curved region may be exerted partly via the mean-flow inhomogeneities which, although not vast in themselves, will tend to lock the spanwise positions of fluctuating vortices.

5.6. *Implications for calculation methods*

As shown in A (see also II) the shear stress inferred from the mean velocity profiles by using standard algebraic formulae for eddy viscosity and mixing length is as much as five times the actual shear stress (for CC30C at $y/\delta = 0{\cdot}5$). Detailed calculations using eddy-viscosity transport equations (e.g. the 'k, ϵ' method) have not yet been done but accurate predictions would require a fivefold increase in the ratio k^2/ϵ compared to an ordinary boundary layer.

Full evaluation of the terms in the Reynolds-stress transport equations from the present results for the concave flows is impracticable because of the large spanwise gradients and the probability that W is non-zero. However values of the generation term $\overline{v^2}\,\partial U/\partial y$ and part of the mean-flow transport term $U\,\partial(-\overline{uv})/\partial x$ in the shear-stress transport equation are given in A for CC30C at $y/\delta = 0{\cdot}5$, to illustrate an estimate of the unmeasured pressure-strain 'redistribution' term which presents one of the main problems in turbulence modelling. The increase in the generation term

between entry (as represented by values at $x = -251$ mm) and $x = 30$ mm is much smaller than the factor of increase in $\overline{v^2}$, because $\partial U/\partial y$ falls by a factor 1·4: downstream of the bend the generation falls rapidly, being only a tenth of the upstream value at $x = 635$ mm (the reduction due to boundary-layer growth on a flat surface would be only about 40 per cent). The streamwise component of the mean-transport term, averaged between $x = -133$ mm and $x = 30$ mm, is about *half* the average generation: $V\partial(-\overline{uv})/\partial y$ is more difficult to estimate, since both factors change greatly within the bend, but is of the same sign as $U\,\partial(-\overline{uv})/\partial x$ although considerably smaller. Thus at least half the generation of shear stress within the bend actually goes into increasing the shear stress and rather less than half is absorbed by the pressure-strain term.

Neglecting turbulent transport normal to the surface, an acceptable approximation near $y/\delta \simeq 0{\cdot}5$, we conclude that the pressure-strain term within the bend (i.e. the difference between generation and mean-flow transport) *averages* only two-thirds of the value at entry (closely equal to the generation term at entry): the minimum value within the bend must be even smaller. This large decrease in the pressure-strain term is all the more remarkable when one recalls that part of the pressure-strain term is closely associated with the mean-velocity gradient $\partial U/\partial y$ and appears to act in direct opposition to the generation: it is somewhat unlikely that this part of the pressure-strain term will decrease markedly when the generation term increases. The remaining parts of the pressure-strain term are that closely associated with the other component of the mean strain rate, $\partial V/\partial x$, and that dependent solely on the fluctuating velocity field. When the flow enters the region of streamline curvature, only the parts of the pressure-strain term that depend on the mean rate of strain can change immediately. The $\partial U/\partial y$-dependent term will decrease by at most 20 per cent because the mean vorticity $\partial V/\partial x - \partial U/\partial y$ remains constant and $\partial V/\partial x$ becomes roughly equal to (and rather smaller than) U/R; we cannot estimate the $\partial V/\partial x$-dependent part, which is initially zero, but it undoubtedly opposes the $\partial U/\partial y$-dependent term in a destabilized flow. As the turbulence structure itself changes, the part of the pressure-strain term that depends only on the fluctuating velocity field will also change (and will almost certainly decrease), while the $\partial U/\partial y$-dependent term may well rise again, following the rise in the generation term. Without measurements of the pressure fluctuations it is not possible to quantify these inferences, but the combined decrease in the $\partial V/\partial x$-dependent term and the fluctuation-dependent term is probably at least as large as the original size of the fluctuation-dependent term.

Estimates of the mean-flow transport term further downstream are likely to be unrealistic because of the above-mentioned three-dimensionality but the collapse in the generation term is undoubtedly accompanied by a collapse in the pressure-strain term. The fact that the shear stress starts to decrease rapidly immediately downstream of the bend suggests that the pressure-strain term does *not* decrease immediately the curvature decreases: the best estimate that can be made suggests a small increase, and the $\partial V/\partial x$-dependent term does of course increase (from its negative value) as $\partial V/\partial x$ goes to zero. Again, the size of the fluctuation-dependent term cannot be assessed, but its reaction time is expected to be of the same order as that of the energy-containing eddies – that is, of order $\delta/(-\overline{uv})^{\frac{1}{2}}$ – so that it will change only slowly.

6. Conclusions

The large changes in turbulence properties that take place in short bends with large turning angle (approximating 'impulses' of curvature), and even the non-monotonic recovery of the properties to their undisturbed values, can be explained qualitatively or semi-quantitatively by existing concepts. Indeed the present results provide an excellent demonstration that the response of turbulence to perturbations is at least of second order (in the sense of control theory) as implied by transport-equation calculation methods. However there are significant changes in the dimensionless structure parameters of the turbulence, which will in general correspond to changes in the 'constants' used in transport-equation modelling. In this experiment we have investigated structure parameters based on double and triple velocity products, and while no simple laws for their variation have emerged some qualitative explanations can be offered.

The various forms of shear-stress parameter, of which the stress/energy ratio is the most relevant to transport-equation modelling, are increased by concave (destabilizing) curvature. The increase in the present experiments was the same for 20 degree and 30 degree turning angles and appeared to be independent of spanwise position. The implication is that saturation values may have been approached: the anisotropy parameter $K \equiv (\overline{u^2} - \overline{v^2})/(\overline{u^2} + \overline{v^2})$ reaches as a high a value at the concave bend exit as it does in a prolonged homogeneous plane strain (about 0·65 in each case, compared with the asymptotic value of unity predicted by rapid distortion theory). However, the increase in dimensional properties such as shear stress shows no sign of saturation and can be roughly predicted by the linear formulae developed for small strain rates. Convex (stabilizing) curvature leads to large reductions in shear-stress parameters, which even reach negative values, and linear formulae are not usable. Downstream of the bends, the shear-stress parameters on the concave side decrease below the upstream values. The reason is not clear; the presence of mean longitudinal vortices may be partly responsible, and since the large eddies at exit from the bend probably contain unusually large longitudinal-vorticity *fluctuations* there may be a period in which these have decayed but the conventional mixing-jet large eddies have not re-formed. On the convex side, the shear-stress parameters return to the upstream values very rapidly, much more rapidly than the shear stress itself.

The most suitable triple-product parameters are the turbulent transport velocities normalized by the free stream velocity (strictly, a turbulent velocity scale should be used; for convenience, we used a reference velocity close to the free-stream velocity). Their response to curvature is in the expected sense and the recovery generally monotonic. The large negative Reynolds-stress gradients that occur near the surface some distance downstream of the concave bends, and in the outward-propagating 'stress bore' downstream of the convex bend, lead to large positive (outward) transport velocities in these regions. By contrast, the large positive stress gradients just downstream of the concave bends do *not* lead to negative transport velocities. It seems probable that transport equations for triple products will be needed in calculation methods for strongly perturbed flows like the present ones; since the transport velocities are much more simply behaved than the triple products themselves, it may be convenient to use simplified equations for the transport velocities as such.

Further work is needed to establish how the strength of the mean vortex pattern

depends on spanwise inhomogeneities upstream of the curved region, and to study large-eddy behaviour by means of conditional sampling techniques.

This work was initiated at the request of the Ministry of Technology, and later supported by the Ministry of Defence (Procurement Executive). We are grateful to Dr P. H. Hoffmann for the data reproduced in figure 6(*b*), obtained during work on longitudinal vortices supported by Brown Boveri et Cie.

REFERENCES

BRADSHAW, P. 1965 *J. Fluid Mech.* **22**, 679.

BRADSHAW, P. 1972 Two more wind tunnels driven by aerofoil type centrifugal blowers. *I. C. Aero Rep.* 72–10.

BRADSHAW, P. 1973 Effects of streamline curvature on turbulent flow. *AGARDograph* 169.

BRADSHAW, P. 1974 *J. Fluid Mech.* **63**, 449.

BRADSHAW, P. 1975 *J. Fluids Engng, Trans. A.S.M.E.* I **97**, 146.

BRADSHAW, P. 1976 Complex turbulent flows. In *Theoretical and Applied Mechanics* (ed. W. T. Koiter), p. 103. North Holland.

BRADSHAW, P. & WONG, F. Y. F. 1972 *J. Fluid Mech.* **52**, 113.

BROWN, G. L. & THOMAS, A. S. W. 1977 *Phys. Fluids* **20**, S243.

CASTRO, I. P. & BRADSHAW, P. 1976 *J. Fluid Mech.* **73**, 265.

CHANDRSUDA, C. 1976 Ph.D. thesis, Imperial College, London.

COLES, D. E. & HIRST, E. A. 1969 *Proc. Computation of Turbulent Boundary Layers*, 1968 *AFOSR–IFP–Stanford Conference*, vol. II, Thermosciences Div. Stanford University.

ELLIS, L. B. & JOUBERT, P. N. 1974 *J. Fluid Mech.* **62**, 65.

FERNHOLZ, H. H. 1962 *Aero. Res. Counc. R. & M.* 3368.

GRANT, H. L. 1958 *J. Fluid Mech.* **4**, 149.

GUITTON, D. E. & NEWMAN, B. G. 1977 *J. Fluid Mech.* **81**, 155.

HOFFMANN, P. H. & BRADSHAW, P. 1978 The response of turbulent boundary layers to mild longitudinal curvature. *Imperial College Aero Rep.* 78–04.

JOHNSTON, J. P., HALLEEN, R. M. & LEZIUS, D. K. 1973 *J. Fluid Mech.* **56**, 533.

KOYAMA, H., MASUDA, S., ARIGA, I. & WATANABE, I. 1979 Stabilizing and destabilizing effects of Coriolis force on two-dimensional laminar and turbulent boundary layers. *J. Engng Power, Trans. A.S.M.E.* **101**, 23.

LEZIUS, D. K. & JOHNSTON, J. P. 1976 *J. Fluid Mech.* **77**, 153.

MERONEY, R. N. & BRADSHAW, P. 1975 *A.I.A.A. J.* **13**, 1448.

PATEL, V. C. 1965 *J. Fluid Mech.* **23**, 185.

RAMAPRIAN, B. R. & SHIVAPRASAD, B. G. 1978 *J. Fluid Mech.* **85**, 273.

SMITS, A. J., EATON, J. A. & BRADSHAW, P. 1978 The response of a turbulent boundary layer to lateral divergence. *Imperial College Aero Rep.* 78–03.

SMITS, A. J., EATON, J. A. & BRADSHAW, P. 1979 *J. Fluid Mech.* **94**, 243.

SMITS, A. J., YOUNG, S. T. B. & BRADSHAW, P. 1978 The effect of short regions of high surface curvature on turbulent boundary layers. *Imperial College Aero Rep.* 78–02.

SO, R. M. S. 1975 *J. Fluid Mech.* **70**, 37.

SO, R. M. C. & MELLOR, G. L. 1972 An experimental investigation of turbulent boundary layers along curved surfaces. *N.A.S.A.* CR–1940.

SO, R. M. C. & MELLOR, G. L. 1975 *Aero. Quart.* **16**, 25.

TOBAK, M. 1971 *Z. angew. Math. Phys.* **22**, 130.

TOWNSEND, A. A. 1976 *The Structure of Turbulent Shear Flow.* Cambridge University Press.